Climate of the Past

Open Access

Discussions

Quantifying molecular oxygen isotope variations during a Heinrich Stadial

C. Reutenauer[1], A. Landais[2], T. Blunier[1], C. Bréant[2], M. Kageyama[2],
M-N. Woillez[2,a], C. Risi[3], V. Mariotti[2], and P. Braconnot[2]

[1]Centre for Ice and Climate, Niels Bohr Institute, University of Copenhagen, Copenhagen, Denmark
[2]Institut Pierre Simon Laplace (IPSL), Laboratoire des Sciences de Climat et de l'Environnement (LSCE), UMR8212 (CEA-CNRS-UVSQ), CE Saclay, Orme des Merisiers, Bat. 701, 91191 Gif-sur-Yvette Cedex, France
[3]Laboratoire de Météorologie Dynamique UMR8539, IPSL/CNRS/UPMC, 4, place Jussieu, 75252 Paris Cedex 05, France
[a]now at: IFPEN, 14 avenue de Bois Préau, 92852 Rueil-Malmaison Cedex, France

Correspondence to: C. Reutenauer (creuten@nbi.dk)

CPD

11, 2281–2339, 2015

$\delta^{18}O$ variations during a HS

C. Reutenauer et al.

Title Page

Abstract	Introduction
Conclusions	References
Tables	Figures

◄◄	►►
◄	►
Back	Close

Full Screen / Esc

Printer-friendly Version

Interactive Discussion

Abstract

δ^{18}O of atmospheric oxygen ($\delta^{18}O_{atm}$) undergoes millennial scale variations during the last glacial period, and systematically increases during Heinrich Stadials (HS). Changes in $\delta^{18}O_{atm}$ combine variations in biospheric and water cycle processes. The identification of the main driver of the millennial variability of $\delta^{18}O_{atm}$ is thus not straightforward. Here, we quantify the response of $\delta^{18}O_{atm}$ to such millennial events using a freshwater hosing simulation (HS_exp) performed under glacial boundary conditions. Our global approach takes into account the latest estimates of isotope fractionation factor for respiratory and photosynthetic processes and make use of atmospheric water isotopes and vegetations changes. Our modeling approach allows to reproduce the main observed features of a HS in terms of climatic conditions, vegetation distribution and δ^{18}O of precipitation. We use it to decipher the relative importance of the different processes behind the observed changes in $\delta^{18}O_{atm}$. The results highlight the dominant role of hydrology on $\delta^{18}O_{atm}$ and confirm that $\delta^{18}O_{atm}$ can be seen as a global integrator of hydrological changes over vegetated areas.

1 Introduction

Oxygen is one of the most abundant species in atmospheric air. As oxygen is produced by photosynthesis and consumed by respiration, a record of oxygen concentration in the past should help us to constrain these two major biospheric fluxes on Earth and potentially provide information on their link with the carbon cycle.

Changes in the O_2/N_2 ratio can be measured in air trapped in ice core back to 800 kyr (Bender, 2002; Kawamura et al., 2007; Landais et al., 2012; Bazin et al., 2014). Unfortunately the O_2/N_2 ratio in ice cores does not provide a direct information on the true atmospheric variations because it is affected by effusion process during bubble formation at pore close-off, roughly 100 m below the ice-sheet surface, and by gas loss during ice core storage. These effects have less impact on the isotopic composition of

oxygen. These isotopic compositions have thus been used to infer information on past biospheric productivity (Luz et al., 1999).

When dealing with isotopes, it is standard to use the isotope ratio, R, defined as the fraction of the abundance of the rare isotope over the dominant one in a substance. Since changes in isotope ratios through natural processes are very small, they are expressed in relation to a standard (recent air and Vienna Standard Mean Ocean Water (VSMOW) being used for O_2 and H_2O respectively) using the δ notation,

$$\delta^{18}O = \frac{^{18}R_{sample}}{^{18}R_{standard}} - 1, \tag{1}$$

$\delta^{18}O$ and $\delta^{17}O$ of atmospheric oxygen have been measured over the past 800 kyr with a mean resolution of about 1500 yrs (e.g. Landais et al., 2010, and references therein; Blunier et al., 2012). As shown by Bender et al. (1994), $\delta^{18}O$ of atmospheric oxygen, noted $\delta^{18}O_{atm}$ hereafter, cannot easily be related to biospheric productivity through photosynthesis and respiration fluxes. $\delta^{18}O_{atm}$ actually reflects for a large part the isotopic composition of the meteoric water. The later is transmitted to the plant through its roots and stems to the leaves where photosynthesis produces oxygen with an isotopic composition close to the isotopic composition in leafwater. Respiration modifies the isotopic composition of atmospheric oxygen in a complex way. While the processes consuming oxygen enrich atmospheric oxygen through a preferential consumption of the lightest molecules, individual biological pathways are associated with a wide range of oxygen fractionations (Helman et al., 2005).

Based on fractionation factors available at the time, Bender et al. (1994) established that the relative proportion of oceanic vs. terrestrial biospheric productivities together with the difference in isotope fractionation over land and ocean were driving the $\delta^{18}O_{atm}$ budget. Several studies built on this idea and interpret the $\delta^{18}O_{atm}$ variations mainly as variations of the oceanic vs. terrestrial biospheric productivities (Hoffmann et al., 2004; Ciais et al., 2012). However, recent measurements have revealed that over all

fractionation associated with oceanic productivity is very similar to its terrestrial counterpart (Hendricks et al., 2004; Eisenstadt et al., 2010), questioning the interpretation of $\delta^{18}O_{atm}$ as an indicator of the relative proportion of oceanic vs. terrestrial biosphere productivity (Luz and Barkan, 2011b).

⁵ Despite the complex interpretation of $\delta^{18}O_{atm}$, several robust features have already been observed highlighting the potential of these measurements. At the orbital scale, $\delta^{18}O_{atm}$ is showing clear variations at a 23 kyr periodicity (Dreyfus et al., 2007). This strong link with precession is probably related to the variations of the hydrological cycle at low latitudes (Bender et al., 1994). Indeed, variations related to the monsoon regime
¹⁰ strongly imprint the isotopic composition of meteoric water as observed in speleothem records (e.g. Wang et al., 2008). They are easily transmitted to the isotopic composition of atmospheric oxygen because the major part of the biospheric productivity, hence photosynthesis, is occurring in the tropics and subtropics.

At the millennial scale, it has recently been shown that $\delta^{18}O_{atm}$ is responding to
¹⁵ the abrupt climate changes of the last glacial period (Landais et al., 2007b; Severinghaus et al., 2009). The references for the millennial scale variability are the stable water isotopes from Greenland ice cores record exhibiting 25 Dansgaard-Oeschger (DO) events during the last glacial period (NGRIP members et al., 2004). A DO event typically exhibits a sawtooth pattern: (i) a cold phase (Greenland Stadial, noted GS
²⁰ hereafter) lasting from centuries to millennia, followed by a warm phase (Greenland Interstadial, GI) starting with (ii) a rapid transition (a few decades) with an amplitude of up to $16 \pm 2.5\,°C$ (Landais et al., 2004; Huber et al., 2006; Kindler et al., 2014) and ending with (iii) a gradual cooling before an abrupt jump towards glacial values.

During the last decade, mechanisms of glacial abrupt events have been investigated
²⁵ using coupled ocean–atmosphere models of varying complexity (e.g. Kageyama et al., 2013; Stouffer et al., 2006). Recent hypotheses often invoke internal variability (Kleppin et al., 2015; Dokken et al., 2013), involving sea-ice atmosphere interactions (e.g. Li et al., 2005, 2010), through ice-albedo feedback and the impact of sea ice cover on regional temperatures by preventing heat exchange between ocean and atmosphere.

However there remains robust evidence from multiple lines of paleoceanographic information, and modeling that millennial scale variability is linked to changes in the AMOC intensity (e.g. Mc Manus et al., 1998), potentially initiated by large freshwater input in the North Atlantic (e.g. Broecker et al., 1990). The supposed key role of the ocean stems in part from the presence of ice rafted debris (IRD, Ruddiman, 1977; Heinrich, 1988) in marine sediments from the North Atlantic region during the largest GS. Such layers document episodes of massive iceberg discharge in the North Atlantic (Heinrich Events) mainly from the Laurentide (H2, H4, H5) and Fennoscandian (H3, H6) ice sheets (Grousset et al., 1993; Guillevic et al., 2014 and references therein). Even if IRD can be recorded for each GS in some northern marine cores of the Atlantic (Elliot et al., 2002), not all GS are associated with a Heinrich event. Heinrich Stadials (noted HS hereafter) are GS associated with a Heinrich event (Baker et al., 2009; Sanchez Goni and Harrison, 2010).

Several aspects of the observed patterns during DO events can be captured through the response of the Earth system to imposed freshwater perturbations in the North Atlantic (Liu et al., 2009; Otto-Bliesner and Brady, 2010; Kageyama et al., 2010; Roche et al., 2010), mimicking Heinrich events. Depending on the background state of the climate (glacial or interglacial, orbital context), of the AMOC, and of the magnitude of the freshwater forcing, these models produce a complete shutdown of the AMOC (HS-like state) or a reduction of the strength of the AMOC (GS-like state) (e.g. Menviel et al., 2014). The injection of freshwater produces in all models a significant cooling of the North Atlantic region. The amplitude of the associated temperature change is probably affected by the simulated change in sea-ice extent and feedbacks between sea-ice and temperature that vary in the different models (Kageyama et al., 2013). These hosing experiments also produce an inter-hemispheric seesaw temperature pattern and associated impacts on the position of the ITCZ (e.g. Dahl et al., 2005; Broccoli et al., 2006; Krebs and Timmermann, 2007; Swingedouw et al., 2009; Cvijanovic and Chiang, 2013) through a modification of the upper part of the thermohaline circulation. Abrupt climate variation associated with the Greenland signal is found down to low latitudes in

numerous terrestrial and marine archives (e.g. Clement and Peterson, 2008). In a large part of the North Atlantic region, the temperature records follow the Greenland signal but with a smaller amplitude both in marine cores (e.g. Bond et al., 1993; Broecker, 2000) and in speleothems (Fleitmann et al., 2009). Concomitant methane excursions and variations in the isotopic composition of the calcite of speleothems in East Asia (e.g. Wang et al., 2001; Cheng et al., 2012) strongly support the fact that these DO events are associated with major reorganization of the tropical water cycle and hence monsoon intensity through a shift of the ITCZ (Chappellaz et al., 2013; Wang et al., 2008; Pausata et al., 2011).

Over this millennial scale variability, high-resolution measurements of $\delta^{18}O_{atm}$ have been obtained in Greenland and Antarctic ice cores (e.g. Guillevic et al., 2014; Landais et al., 2007b, 2010; Severinghaus et al., 2009). We present in Fig. 1 a synthesis of $\delta^{18}O_{atm}$ evolution from the Siple Dome ice core over HSs displayed on Greenland Ice Core Chronology 2005 (GICC05) timescale, using definitions of onset of Rasmussen et al. (2013) for onsets of GS. The $\delta^{18}O_{atm}$ records show a systematic increase in a few kyrs following the onset of a HS (Fig. 2) by around 0.13‰, from +0.08‰ (HS1) to +0.18‰ (HS5). The difference in the slope inflexion at the onset of HS4 and HS5, more pronounced that for HS1, HS2 and HS3, may be due to the long-term trend observed in $\delta^{18}O_{atm}$. Indeed, from 35 to 15 kyr, $\delta^{18}O_{atm}$ exhibits a constant increase, consistent with the build-up of polar ice-sheet, hence enrichment of ocean water in ^{18}O, but remains relatively stable over MIS3 (Fig. 1).

Because of its global character, $\delta^{18}O_{atm}$ should provide a strong added value compared to the different local records of hydrological cycle variations in different continental and marine archives. However, until now, no quantitative, robust interpretation of past variations in $\delta^{18}O_{atm}$ has been established, which limits the use of $\delta^{18}O_{atm}$ as a quantitative indicator for past biospheric production or variations of the hydrological cycle. The aim of this modeling study is thus to provide a quantitative interpretation for the systematic increase in $\delta^{18}O_{atm}$ over HSs. To reach this objective, we propose a global approach incorporating outputs from a general circulation model implemented

Full Screen / Esc

Printer-friendly Version

Interactive Discussion

with water isotopes and focus on the millennial variability of the last glacial period. We follow a modeling approach already developed by Hoffmann et al. (2004). We combine climatic parameters (temperature and humidity), isotopic composition of meteoric water and vegetation repartition and productivity simulated by different models with monthly mean temporal resolution.

In a first section, we describe the general method used to simulate a global $\delta^{18}O_{atm}$ signal. A second part is dedicated to model validation and the third part proposes to quantify the different contributions (hydrology, vegetation, climatic conditions) to the $\delta^{18}O_{atm}$ signal over a HS equivalent.

2 Method

According to Landais et al. (2007b, 2010) and Severinghaus et al. (2009), the millennial variations of $\delta^{18}O_{atm}$ during the last glacial period are driven by shifts in ITCZ modifying the relative humidity distribution and the isotopic composition of meteoric water consumed by terrestrial biosphere. The build-up of atmospheric oxygen involves numerous processes so that we need to consider (i) the worldwide meteoric water isotopic composition, from which ground water is derived, (ii) the worldwide temperature and humidity, from which evaporative enrichment of leaf water $\delta^{18}O$ is calculated, as well as (iii) the worldwide vegetation cover and Gross Primary Productivity, defining the photosyntetically and respiratory active areas that contribute to $\delta^{18}O_{atm}$.

2.1 Oxygen isotopes mass balance model

Oxygen is exchanged with the terrestrial and marine biospheres as well as with the stratosphere. $\delta^{18}O_{atm}$ can thus be expressed as follows:

$$\delta^{18}O_{atm} = \frac{(F_{terr} \cdot \delta^{18}O_{terr} + F_{mar} \cdot \delta^{18}O_{mar})}{(F_{terr} + F_{mar})} - {}^{18}\epsilon_{strat}, \tag{2}$$

Full Screen / Esc

Printer-friendly Version

Interactive Discussion

where $^{18}\varepsilon_{strat}$ represents the stratospheric isotope fractionation caused by photochemical reaction in the stratosphere involving O_2, O_3 and CO_2. F_{terr} and F_{mar} denote O_2 fluxes of gross terrestrial and oceanic productivity, respectively. $\delta^{18}O_{terr}$ and $\delta^{18}O_{mar}$ are the isotopic composition arising from the terrestrial and oceanic realms, respectively. $^{18}\varepsilon_{strat}$ is a small term, 0.3‰ against ∼ 23.8‰ for $\delta^{18}O_{atm}$ with reference to V-SMOW (Luz et al., 2014) and is not assumed to change significantly over a HS because CO_2 level remains relatively stable. We focus mainly on the millennial scale variations of the terrestrial contribution to $\delta^{18}O_{atm}$ signal, i.e. $F_{terr} \cdot \delta^{18}O_{terr}/(F_{terr} + F_{mar})$.

We do not consider the marine influence in a first approach for the following reasons. First, our aim is to test the hypothesis of Landais et al. (2007a) and Severinghaus et al. (2009) that $\delta^{18}O_{atm}$ millennial scale variations are driven by variations in the low latitudes hydrological cycle through changes in the $\delta^{18}O$ of precipitation. Second, Hendricks et al. (2004) and Luz and Barkan (2011a) have shown that the difference between $\delta^{18}O_{terr}$ and $\delta^{18}O_{mar}$ is not significant. Finally, the spatial and temporal variations of water $\delta^{18}O$ and respiration pathways in the ocean are expected to be relatively small compared to the variations on land, which render their integration for $\delta^{18}O_{atm}$ modelling less crucial as illustrated in the study of Hoffmann et al. (2004).

2.2 Calculation of $\delta^{18}O_{terr}$

The major source of atmospheric oxygen from the terrestrial biosphere is the oxygen produced during photosynthesis. The fractionation associated with photosynthesis is small (Guy et al., 1993; Eisenstadt et al., 2010). The oxygen produced by this process has thus almost the same isotopic composition than the leaf water. Consumption of oxygen is also associated with biosphere productivity through different pathways (dark respiration, photorespiration, Mehler reaction). $\delta^{18}O_{terr}$ thus results from isotope fractionation associated with photosynthesis and oxygen uptake. Following Bender et al. (1994); Blunier et al. (2002); Hoffmann et al. (2004); Landais et al. (2007a), we assume

a steady-state, where photosynthesis equals respiration. $\delta^{18}O_{terr}$ calculates as:

$$\delta^{18}O_{terr} = \frac{(\delta^{18}O_{lw} + 1)}{^{18}\alpha_{resp}} - 1, \tag{3}$$

where $\delta^{18}O_{lw}$ is the global isotopic composition of leaf water and $^{18}\alpha_{resp}$ is the global apparent respiratory isotope fractionation factor associated with global oxygen uptake,

5 i.e. oxygen consumption weighted average of fractionation factors associated with specific respiratory pathways.

2.3 Photosynthetic oxygen

As classically done, we estimate the value of $\delta^{18}O$ of leaf water, hereafter $\delta^{18}O_{lw}$, based on Craig and Gordon (1965) equation (C&G) of evaporation applied to leaf tran-

10 spiration (Dongmann, 1974; Flanagan et al., 1991b). It is thus calculated in the following way:

$$\delta^{18}O_{lw} = h \cdot (\delta^{18}O_{vap} + {}^{18}\varepsilon_{eq}) + (1 - h) \cdot (\delta^{18}O_{gw} + {}^{18}\varepsilon_{eq} + {}^{18}\varepsilon_{kin}), \tag{4}$$

where h is the relative humidity at the site of photosynthesis, $^{18}\varepsilon_{eq}$ is the liquid vapor equilibrium isotope effect dependent of temperature (Majoube, 1971), $^{18}\varepsilon_{kin}$ is the ki-

15 netic isotope effect occurring when humidity is below saturation, $\delta^{18}O_{gw}$ is the isotopic composition of soil water and $\delta^{18}O_{vap}$ is the water vapor $\delta^{18}O$ near the surface. $^{18}\varepsilon_{kin}$ is deduced from the ratio of the diffusion coefficient associated with $H_2^{16}O$ (D) and $H_2^{18}O$ (D*). Several values for the ratio D/D^* can be found in the literature (Merlivat, 1978; Cappa et al., 2003; Luz et al., 2009), varying from 1.028 to 1.032. For leaf water evap-

20 oration, many studies have reported lower enrichment in $\delta^{18}O_{lw}$ than that predicted by Eq. (4) with $^{18}\varepsilon_{kin} = D/D^* - 1$ as classically assumed (e.g. Allison et al., 1985; Bariac et al., 1989; Walker et al., 1989; Walker and Brunel, 1990; Yakir et al., 1990; Flanagan

Discussion Paper | Discussion Paper | Discussion Paper | Discussion Paper | Discussion Paper |

CPD

11, 2281–2339, 2015

$\delta^{18}O$ variations during a HS

C. Reutenauer et al.

Title Page

Abstract   Introduction

Conclusions   References

Tables   Figures

◄   ►I

◄   ►

Back   Close

Full Screen / Esc

Printer-friendly Version

Interactive Discussion

et al., 1991b, a, 1993, 1994). Farquhar et al. (1989) suggested that $^{18}\epsilon_{kin}$ depends on the importance of either stomatal or boundary layer resistances. In moist conditions, stomata resistance is low and boundary layer resistance high, leading $^{18}\epsilon_{kin}$ to value as low as 19‰ when using Merlivat (1978) value for D/D^*. In this study, we have imposed a mean value for $^{18}\epsilon_{kin}$ of 20‰, higher values leading to too high global values for $\delta^{18}O_{atm}$.

The calculation of $\delta^{18}O_{lw}$ using Eq. (4) requires spatial and temporal variations of temperature and relative humidity as well as the variations of the isotopic composition of water vapor and meteoric water, from which $\delta^{18}O_{gw}$ will be deduced (Sect. 2.3.2). These variables are obtained from outputs of modeling experiments.

2.3.1 Simulated climatic variations over an abrupt cooling

For inferring temperature and relative humidity variations over a HS, we have used the atmosphere–ocean general circulation model (AOGCM) IPSL_CM4 (Marti et al., 2010) with a resolution for the atmosphere grid of $96 \times 72 \times 19$ in longitude × latitude × altitude. As stated above, to model $\delta^{18}O_{atm}$ we have used the simulation of a HS achieved from a freshwater hosing experiment run in glacial conditions in a coupled general circulation model. We will thus compare in the following the outputs of two simulations: one for the Last Glacial Maximum (LGM_ctrl) and one for the Heinrich Stadial (HS_exp).

The glacial boundary conditions are as follows (see Kageyama et al., 2009 for a detailed presentation of the climate setup): orbital parameters for 21 kyBP, CO_2, CH_4 and N_2O levels set to 185 ppm, 350 and 200 ppb respectively (Monnin et al., 2001; Dällenbach et al., 2000; Flückiger et al., 1999), ICE-5G ice-sheet reconstruction (Peltier, 2004).

The first experiment is an equilibrated glacial run (LGM_ctrl) used as reference run (see LGMb in Kageyama et al., 2009). The second experiment (HS_exp) is a water hosing experiment, where an additional freshwater flux of 0.1 Sv ($1\,Sv = 10^6\,m^3\,s^{-1}$) is imposed instantaneously in the Atlantic North of 40° N and the Arctic (see LGMc

in Kageyama et al., 2009) from year 150 of the reference run until year 550 of the reference run. The input of freshwater in HS_exp, mimicking a Heinrich event, leads to an AMOC collapse in 250 years (see Fig. 1a in Woillez et al., 2013).

The climate response to the AMOC collapse in the HS_exp is of global extent and qualitatively agrees with paleoarchives reconstructions for the North-Atlantic cooling, southwards Atlantic ITCZ migration and weakening of Indian and African monsoons (Kageyama et al., 2009, 2013). However, the model does not simulate an Antarctic warming or weakened East Asian Monsoon (noted EASM hereafter) (Kageyama et al., 2009). In the following we used the monthly-averaged spatial fields of temperature and humidity calculated on the coupled model grid. From these data we followed Lloyd and Farquhar (1994) approach to link leaf temperature during photosynthesis, Tp, to monthly temperature in the first layer of the model, Tm, through Tp = 1.05 · (Tm + 2.5). 2.5 °C are added to Tm to account for the daytime increase in air temperature at the time of photosynthesis. The 5 % increase allows for net canopy to air heat fluxes (Farquhar and Lloyd, 1993). The relative humidity from the first layer is not modified (Farquhar et al., 2007).

2.3.2 Modeling of δ^{18}O of meteoric water and groundwater

For our estimate, we also need the distribution of the oxygen isotopic composition of meteoric water. We extract it from the isotopic version of the atmospheric general circulation model developed at the Laboratoire de Météorologie Dynamique (LMDZ4) (Risi et al., 2010). LMDZ is the atmospheric component of the IPSL-CM4 model used above. The monthly sea surface temperature and sea ice fields obtained from the two aforementioned experiments at equilibrium (LGM_ctrl and HS_exp) have been used as surface boundary conditions for the isotopic simulations.

We present on Fig. 3 the mean annual δ^{18}O of precipitation, noted $\delta^{18}O_p$ hereafter, simulated for the LGM_ctrl and the HS_exp experiments. The $\delta^{18}O_p$ repartition for the

LGM_ctrl experiment has already been confronted to data for validation in Risi et al. (2010).

In HS_exp, we observe a general decrease of $\delta^{18}O_p$ compared to the $\delta^{18}O_p$ in the LGM_ctrl experiment. For validation purpose, $\delta^{18}O_p$ changes are compared with changes in (i) calcite $\delta^{18}O$ in speleothems, noted $\delta^{18}O_c$ hereafter, and in (ii) ice $\delta^{18}O$ in Greenland ice cores over Heinrich events (Sect. 3.1.2, see Fig. 4a for $\delta^{18}O_p$ anomaly).

Finally Eq. (4) also requires an estimate of $\delta^{18}O_{gw}$. Groundwater pumped through the plant's roots represents a mixture of stored water and incoming precipitation water (McGuire et al., 2002). Indeed, during spring/summer when maximal productivity occurs the groundwater is composed of significant amounts of fall/winter precipitation. In order to take the mixing into account we use amount-weighted annual-mean $\delta^{18}O$ of precipitation. This approach has been shown to be realistic in a field experiment in Kenya (Wang et al., 2012) and has been implemented in global coupled climate model of intermediate complexity (Caley et al., 2014). Doing so, we neglect the fractionation effects that can significantly affect the soil water isotopic composition, especially in dry regions (Kanner et al., 2014).

2.4 Oxygen uptake in respiratory processes

2.4.1 Global oxygen production

The geographical distribution of respiratory O_2 fluxes (noted GPP_O_2 hereafter from the hypothesis of equilibrium between oxygen production and consumption) is computed from the vegetation cover and Gross Primary Productivity (GPP) distribution provided by the ORCHIDEE model which simulates the vegetation distribution of 10 natural plant functional types (PFT) (Krinner et al., 2005). ORCHIDEE is the land surface component of the IPSL-CM4 model. It is used here with the same spatial resolution as the aforementioned models (latitude × longitude 3.75° × 2.5°) and is run in offline mode, forced by the high-frequency outputs from IPSL-CM4_v1 for the two ex-

$\delta^{18}O$ variations during a HS

C. Reutenauer et al.

periments LGM_ctrl and_HS_exp. The prescribed forcing has a 6 h time-step temporal resolution, and thus takes into account daily variability and diurnal cycle simulated by the IPSL model (Woillez, 2012). Each grid cell simulates the vegetation cover by splitting the cell into fractions of 10 Plant Functional Types (PFT, see Table 1 for names)

5 and provides GPP fluxes ($gC m^{-2} yr^{-1}$) for each PFT. Validation of the vegetation cover can be found in Woillez et al. (2011) for LGM_ctrl and Woillez et al. (2013) for HS_exp over Western Europe. Here we extend this work and compare LGM and HS simulation with worldwide vegetation reconstructions selected from marine (coastal) and terrestrial paleoarchives with high temporal resolution (Sect. 3.1.3).

10 In this study, following Hoffmann et al. (2004), we calculate the terrestrial biosphere's O_2 fluxes in 3 steps. First, the outputs from ORCHIDEE provide the GPP expressed in $gC m^{-2} yr^{-1}$ for each of the 10 PFT's on each model grid point. Second, simulated carbon molar fluxes for each PFTs are converted to oxygen molar fluxes, based on the biochemical model of photosynthesis from Farquhar et al. (1980). The model ac-

15 counts for fraction of photorespiration and the photosynthetic quotient (PQ) -measured by Keeling (1988) and Severinghaus (1995) as ~ 1.1. Third, GPP_O_2 for each PFT is expressed in terms of dark respiration (mitochondrial), Mehler respiration and photorespiration, each of these respiratory uptake processes being associated with a specific fractionation (refer to Table 2 for values):

20
$$\text{GPP\_}O_2 = \text{GPP\_}O_2\text{\_Mehler} + \text{GPP\_}O_2\text{\_dark} + \text{GPP\_}O_2\text{\_photo} \qquad (5a)$$
$$= \frac{\text{GPP} \cdot \text{PQ} \cdot (1 + f_{\text{photo}})}{1 - f_{\text{Mehler}}},$$

With,
$$\text{GPP\_}O_2\text{\_Mehler} = f_{\text{Mehler}} \cdot \text{GPP\_}O_2, \qquad (5b)$$
$$\text{GPP\_}O_2\text{\_dark} = (1 - f_{\text{Mehler}}) \cdot \text{PQ} \cdot \text{GPP}, \qquad (5c)$$
25
$$\text{GPP\_}O_2\text{\_photo} = (1 - f_{\text{Mehler}}) \cdot (\text{GPP\_}O_2 - \text{PQ} \cdot \text{GPP})$$
$$= (1 - f_{\text{Mehler}}) \cdot \text{PQ} \cdot \text{GPP} \cdot f_{\text{photo}}, \qquad (5d)$$

where f_{Mehler} denotes the fraction of Mehler reaction, and accounts for 10 % of the total respiration (Badger et al., 2000) and f_{photo} represents the fraction of photorespiration.

2.4.2 Photorespiration

All types of C3 plants photorespire, but in different proportions. In contrast, C4 plants do
5   not photorespire, because of a CO_2 concentration mechanism allowing them to operate at high chloroplast CO_2 partial pressures and thereby to inhibit the oxygenation reaction during photosynthesis (Von Caemmerer, 2000). The proportion of photorespiration, f_{photo}, depends thus on the type of plants (10 PFT's in this study), on the atmospheric concentration of CO_2 (taken constant in this study) and on temperature. Details on
10   equations used in our offline model for $\delta^{18}O_{terr}$ calculation can be found in Hoffmann et al. (2004).

2.4.3 Global terrestrial fractionation factor

Uptake of oxygen by respiration discriminates against heavy isotopes, leaving the substrate oxygen, atmospheric O_2, enriched in ^{18}O. Each of the oxygen uptake processes
15   is affected by a specific, spatially and temporally constant fractionation (Table 2) and the global terrestrial isotope fractionation factor $^{18}\alpha_{resp}$ is expressed as follows:

$$^{18}\alpha_{resp} = {}^{18}\alpha_{photo} \cdot f_{photo} + {}^{18}\alpha_{Mehler} \cdot f_{Mehler} + {}^{18}\alpha_{dark\_soil} \cdot f_{dark\_soil} \quad (6)$$
$$+ {}^{18}\alpha_{dark\_leaves} \cdot f_{dark\_leaves},$$

The latest estimations of $^{18}\alpha_{Mehler}$, $^{18}\alpha_{photo}$ and $^{18}\alpha_{dark\_leaves}$ can be found in Table 2.
20   A significant proportion of terrestrial respiration (30 to 40 %) occurs below the surface (Raich and Potter, 1995) with varying fractionation values. Respiration below surface ($^{18}\alpha_{dark\_leaves}$) thereby needs to be considered for the different types of soils (boreal, temperate, tropical), as each soil type is associated with a specific fractionation factor because of different diffusion pathways (Angert et al., 2003). Mehler fraction, f_{Mehler},

represents 10 % of global respiration (Badger et al., 2000) and f_{photo} is calculated from the outputs of the ORCHIDEE and IPSL-CM4 models. Dark respiration fraction is composed of leave (38 %) and soil (62 %) respiration, following Landais et al. (2007a).

3 Results

3.1 Simulation of regional climate, vegetation and isotopic pattern during a HS

We propose here a model–data comparison on a regional scale to evaluate the model performances, as the climatic and water cycle responses during a HS are not spatially homogeneous. While the climatic outputs of the HS experiments are already discussed in Kageyama et al. (2009) and Woillez et al. (2013), we discuss the simulated change in relative humidity (Sect. 3.1.1) since the latter has an important influence on the $\delta^{18}O_{lw}$ and hence $\delta^{18}O_{terr}$. Then, we further compare the modeled change in $\delta^{18}O$ of precipitation over a HS with changes in speleothems calcite $\delta^{18}O$ (Sect. 3.1.2) and modeled fraction of vegetation with vegetation reconstructions (Sect. 3.1.3).

3.1.1 Simulated humidity validation

According to climate reconstructions, during HS, wet periods in northeastern Brazil are synchronous with periods of weak East Asian summer monsoons (Wang et al., 2001) and with cold periods in Greenland (Grootes and Stuiver, 1997) and Europe (Genty et al., 2003). Reorganization in tropical rainfall patterns leads to wetter conditions in southwestern North America (Asmerom et al., 2010) and southern South America (Kanner et al., 2012), and to dryer conditions in the Australian-Indonesian monsoon region (Mohtadi et al., 2011), wide parts of Asia (Wang et al., 2008), Northern South America (Peterson and Haug, 2006), Mediterranean region (Fleitmann et al., 2009), and equatorial western Africa (e.g. Weldeab, 2012).

During HS, the model simulates similar humidity patterns as reconstructed ones, with dryer conditions over Europe, the Mediterranean region, Northern and Equatorial Africa, South and East Asia, Middle East, India, southern Australia and parts of Indonesia. In South America, a region of particular interest, where major simulated changes in vegetation and oxygen production occur, the model captures well the observed contrast with increased moisture in Northeastern Brazil, and drying in Northern South America and Central America.

These rapid comparisons show that there is a good general agreement between modeled changes in humidity over an HS and climatic reconstructions over the different regions.

3.1.2 Simulated amount-weighted $\delta^{18}O_p$ validation

Tropics

Comparisons of modeled hosing-driven amount-weighted $\Delta\delta^{18}O_p$ anomalies with reconstructed $\Delta\delta^{18}O$ of speleothem's calcite during HSs are presented in Table 3 and Fig. 4. Thirteen Heinrich $\Delta\delta^{18}O_p$ proxy-reconstructions arise from Lewis et al. (2010) ($n = 11$) and Pausata et al. (2011) ($n = 4$), located in the Eastern Mediterrannean (EM), South American Monsoon (SASM), EASM and Indian Summer Monsoon (ISM), North American Monsoon (NAM) and the Australian-Indonesian Monsoon (AIM) regions. Those regions represent the most productive ones and therefore carry a substantial part of $\delta^{18}O_{terr}$ signal. Although reconstructed $\Delta\delta^{18}O_p$ from Lewis et al. (2010) and Pausata et al. (2011) studies were estimated differently, they are consistent and common reconstructed $\Delta\delta^{18}O_p$ estimates (for Hulu and Songjia cave) are similar in both studies (Table 3, this study; method section of Pausata et al., 2011).

The dominant hydrological controls on reconstructed $\delta^{18}O_p$ are site specific and are described by Lewis et al. (2010). Figure 4 demonstrates the ability of the AGCM LMDZ-iso to reproduce the observed $\Delta\delta^{18}O_p$ spatial pattern for most of the sites, particularly in regions strongly affected by ITCZ variations and hence by changes in the water

Full Screen / Esc

cycle, regardless of the processes at play. There are two regions where the model does not properly reproduce the observed signal over HS. The first one occurs in the ISM domain (Timta Cave). This disagreement can be due to a model bias in a region where the coarse model resolution does not allow to properly represent the role of orography. Indeed, model and observation would reconcile 2 gridcells south of Timta cave, as it is located just at the transition between a positive and negative simulated $\delta^{18}O_p$ anomaly. Another mismatch occurs in the NAM domain (Cave of the Bells), where the observed $\Delta\delta^{18}O_p$ (−0.8‰) and the modeled $\Delta\delta^{18}O_p$ (0.9‰) are of opposite sign. Elevation of the site (1700 m a.s.l.) might explain the disagreement between model and data.

In conclusion, the key features of HS precipitation inferred from speleothem's $\delta^{18}O_c$, i.e. a low latitude inter-hemispheric see-saw pattern (Cheng et al., 2012), with a weakened Asian Monsoon and increased SASM as prominent feature, are generally well captured by the LMDZ model.

High latitudes

In Greenland, HS can hardly be distinguished from the GS or from the mean LGM state. The only clear $\delta^{18}O_{ice}$ signal is observed from GI to GS (or HS) with an approximately 4‰ decrease in central Greenland sites (GRIP, GISP2, NGRIP). The depletion simulated in Greenland, with a 1.6‰ decrease at GRIP site, by the model for a HS compared to a glacial background state is thus consistent with available data.

3.1.3 Validation of simulated vegetation

In order to compare easily model and data, simulated PFT's are gathered into 5 megabiomes (boreal, temperate and tropical trees, C3 and C4 grasses) as well as bare soil. We distinguish among C3 and C4 plants as their partitioning has a strong impact on photorespiration fraction. The simulated dominant vegetation fraction is shown for LGM_ctrl (Fig. 5) and HS_exp (Fig. 6), together with pollen-based reconstructed mega-

biomes. Given its domination, we display bare soil fraction only if it covers more than 80 percent of a gridcell.

LGM_ctrl vegetation

The main features of the glacial vegetation are correctly reproduced by ORCHIDEE model, as briefly presented by Woillez et al. (2011): reduced fractions of tropical forest, particularly in Amazonia, and high grass fractions in Siberia, Alaska, western North-America. Main biases are an overestimation of the tree fractions over Western Europe, eastern Eurasia and eastern North America, as well as an overestimation in bare soil fractions over India, southern Africa and South-America (Woillez et al., 2011).

The model simulates temperate trees in southern East Asia (Vietnam, Southern China, Cambodia), tropical trees and grasses over the western pacific warm pool (Malaysia, Thailand, Indonesia) and over southern Africa, in agreement with BIOME6000 reconstructions (Prentice et al., 2000). The model underestimates temperate trees in Asia and overestimates bare soil in South Africa.

A more detailed comparison shows that the important (boreal) tree fraction over southern Western Europe differs from palynological reconstructions depicting an important grass fraction, but this bias mainly comes from the overestimation of BoBS, which is a common feature in the version of ORCHIDEE used here, also found in present-day vegetation simulations. The bias might also be the sign that the LGM climate simulated by IPSL-CM4 over western Europe is too warm and wet (Woillez et al., 2011). In a few regions, ORCHIDEE correctly simulates the presence of forest, but the dominant type of tree disagrees with pollen reconstructions: tropical trees over Papua-New-Guinea and western Indonesia, while reconstructions reveal the presence of temperate trees over these regions. Simulated forests over southern Australia (a thin coastal band in the South-East) are composed of temperate and tropical trees, while reconstructions rather indicate the presence of a few tropical trees. The model simulates mixed vegetation composed of grasses, boreal and temperate trees in eastern North-America, consistent with pollen data, but the spatial distribution is incorrect.

It is important to keep in mind that model data comparison of vegetation can only remain qualitative given the coarse resolution of the vegetation model, related to the model resolution of the climatic forcing fields. Besides, pollen records represent the surrounding vegetation distribution at different altitudes, while ORCHIDEE model does not account for elevation changes within a grid cell (Woillez et al., 2013).

HS_exp vegetation

To validate the simulated HS vegetation, we compare the millennial-scale changes in selected high resolution (< 800 yr, mean resolution is 400 yr) pollen records of 48 sites described for HS1-GS2 ($n = 16$) in South-America and southern Africa (Hessler et al., 2010; Handiani et al., 2012), and for HS4-GS9 ($n = 31$) in Europe (Fletcher et al., 2010), North-America (Jimenez-Moreno et al., 2010), Japan (Takahara et al., 2010) and Australasia (Harrison and Goni, 2010). Figure 7 displays the location of paleo records discussed in this study. Table 4 summarizes the model–data comparison at a gridcell level and provides additional information revealed by palynological reconstructions. The sampling resolution for the analysed period (MIS2 for HS1, MIS3 for HS4), the other biomes represented for a given site and the potential occurrences of similar reconstructed vegetation changes over other HS's are presented.

The model–data comparison has been performed as follows: the 2 dominant reconstructed biomes are compared with the 2 dominant simulated biomes over the gridcell covering the site where the proxy originates. Among the 48 sites with pollen reconstructions, 12 of them were discarded because of absence of vegetation on the considered gridcell. Among the 36 terrestrial and coastal sites, 11 disagree (30 %) and 25 (70 %) of them display a moderate to good agreement (Table 4). A good agreement ($n = 13$) is obtained when reconstructed and simulated dominant biomes are alike, a fair agreement ($n = 9$) when a subdominant biome agrees with a dominant one, and a moderate agreement ($n = 3$) when subdominant biomes only are similar.

Simulated vegetation in regions associated with high oxygen productivity agrees well with pollen reconstruction. This is the case for South America, where a strong increase

of tropical forest at the expense of bare soil is simulated in Eastern Brazil, or in the West Pacific Warm Pool region, where tropical forest represents the dominant biome. The slight southward shift of the southern border of desert areas in Equatorial Africa is also well captured by ORCHIDEE. In the ISM region, the simulated weakened monsoon (Kageyama et al., 2009) leads to the appearance of desert areas south and east of India, consistent with a dryer climate revealed by a core from the Indus region (Deplazes et al., 2014).

From this analysis it appears that sites showing a disagreement between model and data are either coastal sites and/or have a very high bare soil fraction. Coastal sites do not necessarily only represent the vegetation in the coastal region, but they offer numerous records and allow high-resolution analysis thanks to their high sedimentation rate, so it is crucial to include them for millennial scale analysis. 5 (50 %) of the sites showing no agreement present a very high simulated bare soil fractions (> 90 %). Woillez et al. (2013) already pointed out the overestimation of bare soil fractions by ORCHIDEE model. We argue that this bias might partly explain the observed discrepancy between model and data. Besides, the other sites showing a disagreement, over Europe and Australia, underestimate grass fraction. For Europe, the bias is already present in the LGM simulation and is probably partly due to the systematic overestimation of forest by ORCHIDEE in this region (Woillez et al., 2011). Given the scarcity of data offering a time resolution high enough to catch millennial-scale vegetation variability, further testing of the simulated vegetation remains challenging. In conclusion, HS_exp vegetation agrees reasonably well with available pollen based vegetation reconstruction.

Finally, based on the reasonable agreement of the simulated changes in vegetation, humidity and precipitation with observations depicted in this section, we can rely on the validity of the model to simulate $\delta^{18}O_{terr}$ over a HS.

3.2 Global increase $\delta^{18}O_{terr}$ during a HS

The model calculates $\delta^{18}O_{terr}$ for LGM_ctrl and HS_exp as 23.41 and 23.52‰, respectively (Table 2). This average $\delta^{18}O_{terr}$ value is coherent with the $\delta^{18}O_{atm}$ value of 23.8‰ with respect to V-SMOW and the finding that terrestrial and marine contribution to $\delta^{18}O_{atm}$ are similar (Luz et al., 2014). Moreover, the global increase in $\delta^{18}O_{terr}$ of 0.11‰, (Fig. 8) can quantitatively explain most of the 0.1‰ $\delta^{18}O_{atm}$ increase over HS (Severinghaus et al., 2009; Guillevic et al., 2014) (Fig. 1). In the following, we use the different model outputs to decipher the main influences on $\delta^{18}O_{terr}$ and hence on $\delta^{18}O_{atm}$.

By construction (Eq. 3), $\delta^{18}O_{terr}$ is linearly dependent on both $\delta^{18}O_{lw}$ and $^{18}\varepsilon_{resp}$, so that we discuss these two effects below. Figure 8 (upper panel) details the different contributions to $\delta^{18}O_{terr}$ change over a HS and demonstrates the dominant role of $\delta^{18}O_{lw}$ (Sect. 3.2.1) compared to $^{18}\varepsilon_{resp}$ (Sect. 3.2.2). Indeed, the 0.11‰ increase in $\delta^{18}O_{terr}$ exclusively stems from $\delta^{18}O_{lw}$ increase (+0.14‰ over HS_exp), while respiratory fractionation leads to a negative anomaly (−0.03‰) over HS_exp. We explore in more details below the origin of the relative changes in $^{18}\varepsilon_{resp}$ and $\delta^{18}O_{lw}$ as calculated by our modelling approach. In particular, we look at the different regional contributions to the global $^{18}\varepsilon_{resp}$ and $\delta^{18}O_{lw}$ signals since low latitude regions are associated with the largest GPP_O$_2$ (Fig. 9a) and hence have the strongest influence on the global $\delta^{18}O_{terr}$ signal (Fig. 9c).

3.2.1 Leafwater

We find global $\delta^{18}O_{lw}$ values of 5.16 and 5.30‰ for LGM_ctrl and HS_exp, respectively. The 0.14‰ difference is similar to the $\delta^{18}O$ increase observed in ice cores during HS (Fig. 2). The increase of $\delta^{18}O_{lw}$ is clearly visible in the low latitude regions and explained by the combined effects of an increase in $\delta^{18}O_p$ and a decrease in GPP_O$_2$ weighted relative humidity (Fig. 9b). $\delta^{18}O_{lw}$. Still, when looking at the global budget, the

GPP_O$_2$ weighted relative humidity is not significantly different in HS and in LGM state. This is due to the decrease in relative humidity during HS in the extra-tropical regions (Fig. 9b). The net effect of relative humidity on δ^{18}O$_{lw}$ is thus nil. As a consequence, the main driver of δ^{18}O$_{lw}$ (and hence on δ^{18}O$_{terr}$) increase is the increase in GPP_O$_2$ weighted δ^{18}O$_p$ (Fig. 9b) by 0.18‰ (Fig. 8). This increase is linked to the southward shift of the tropical belt occurring during HS, as suggested from the speleothem data compilation (see Sect. 3.1.2).

3.2.2 Respiration

Respiratory processes lead to a 0.03‰ decrease of δ^{18}O$_{terr}$ in HS_exp compared to δ^{18}O$_{terr}$ in LGM_ctrl (Fig. 8a),. This variation is too small to challenge δ^{18}O$_{terr}$ enrichment caused by hydrological processes. Here we explain the stability of $^{18}\varepsilon_{resp}$ on millennial timescales by a compensatory mechanism taking place between the main respiratory pathways.

$^{18}\varepsilon_{resp}$ is classically separated into 4 contributions as given in Eq. (6): soil respiration, leaf respiration, photorespiration and Mehler reaction.

Soil respiration with associated fractionation factor $^{18}\alpha_{dark\_soil}$ represents 63 % of dark respiration (Schlesinger and Andrews, 2000). It represents 39 % of global terrestrial respiration in our simulation, in agreement with estimates from Raich and Potter (1995) of 30 to 40 %. $^{18}\alpha_{dark\_soil}$ is temperature dependent (Angert et al., 2003), with higher fractionation associated with colder soils, causing a high zonal contrast. This temperature effect leads to a change of $^{18}\alpha_{dark\_soil}$ by 0.28‰ over HS, increasing $^{18}\varepsilon_{resp}$ by 0.12‰ and in turn depleting δ^{18}O$_{terr}$.

Photorespiration fraction, strongly discriminative against ^{18}O ($^{18}\alpha_{photo} = -21.4$‰), represents 28.56 % of the global terrestrial oxygen uptake in LGM_ctrl. The proportion of photorespiration is mainly linked to the change in the C3 vs. C4 plant proportions and in temperature during photosynthesis (Von Caemmerer, 2000; Hoffmann et al., 2004). During HS_exp, photorespiration fraction increases by 1 % (29.52 %), driven by

a slight decrease in C4 grass (1.3 %) and a slight photosynthesis temperature increase (0.3 °C). As a result, $^{18}\varepsilon_{\mathrm{resp}}$ decreases by 0.04 ‰ in HS_exp, thus causing $\delta^{18}O_{\mathrm{terr}}$ enrichment.

Summarizing, in high latitudes, cold temperatures lead to a weak photorespiration but strong soil isotope fractionation. In low latitudes, high temperatures and variable C4 fraction lead to a weak soil isotope fractionation and a highly variable photorespiration. This compensatory mechanism between photorespiration and soil respiration fractionations explains thus the minor role of respiration in $\delta^{18}O_{\mathrm{terr}}$ anomaly during HS.

4 Discussion

Our results suggest a strong control of tropical hydrology on $\delta^{18}O_{\mathrm{terr}}$ through changes in $\delta^{18}O_{\mathrm{p}}$. It suggests that $\delta^{18}O_{\mathrm{atm}}$ is very strongly related to tropical hydrology and may be a good tracer for global monsoon signal. The aim of the following discussion is to evaluate these results by (i) providing some insights on $\delta^{18}O_{\mathrm{mar}}$ estimate and (ii) testing the robustness of our conclusion on the driver of $\delta^{18}O_{\mathrm{terr}}$ changes through 3 sensitivity experiments separating the different parameters (hydrology, climate and vegetation).

4.1 Estimate of $\delta^{18}O_{\mathrm{mar}}$ over a Heinrich Stadial

$\delta^{18}O_{\mathrm{mar}}$ has been recently estimated as 24.3 ± 2.0 ‰ for present day (Luz et al., 2014). In order to estimate $\delta^{18}O_{\mathrm{mar}}$ for LGM and HS, we assumed that fractionation during oxygen uptake by marine biosphere remained constant between LGM/HS and present-day and used a mean ocean $\delta^{18}O$ enriched by 1 ‰ at LGM (Waelbroeck et al., 2002). This results in a value of $\delta^{18}O_{\mathrm{mar}}$ of 25.3 ± 2.0 ‰ for LGM and HS. It is important to note that a rise in sea level during a HS would lead to a depleted mean ocean $\delta^{18}O$, as polar ice sheet accumulate ^{16}O, and can therefore not explain the increased $\delta^{18}O_{\mathrm{atm}}$ observed during stadials.

Discussion Paper | Discussion Paper | Discussion Paper | Discussion Paper |

CPD

11, 2281–2339, 2015

$\delta^{18}O$ variations during a HS

C. Reutenauer et al.

Title Page

Abstract | Introduction

Conclusions | References

Tables | Figures

|◄ | ►|

◄ | ►

Back | Close

Full Screen / Esc

Printer-friendly Version

Interactive Discussion

Because of the spatial limitation of paleo-records to provide a global picture of marine primary productivity, we have estimated the marine productivity for LGM and HS by the Pelagic Interaction Scheme for Carbon and Ecosystem Studies (PISCES) model. PISCES model is a biogeochemical model of the global ocean including a simple representation of marine ecosystem and forced offline by the AOGCM IPSL-CM4 (Aumont and Bopp, 2006; Mariotti et al., 2012). The model PISCES has already been compared under glacial conditions with observations (Mariotti et al., 2012; Tagliabue et al., 2009; Bopp et al., 2003) and reproduces roughly the paleoproductivity reconstruction of Kohfeld et al. (2005). Using the same forcings as for our simulations, Mariotti et al. (2012) simulate a global decrease of oceanic primary productivity of 16 % during a Heinrich event, in agreement with independent modeling studies (Schmittner, 2005; Menviel et al., 2008; Schmittner and Galbraith, 2008) and more important that the one in terrestrial GPP (3.5 %). Because $\delta^{18}O_{mar}$ is larger than $\delta^{18}O_{terr}$, this decrease in marine productivity would lead to a decrease in global $\delta^{18}O_{atm}$ during the HS, opposite to the observation. We conclude that marine productivity is not the driver for $\delta^{18}O_{atm}$ increase during HS.

4.2 Disentangling the influences of climate, hydrology and vegetation on $\delta^{18}O_{atm}$: sensitivity experiments.

In order to assess the robustness of our conclusion stating that low latitude hydrological cycle is the driver of $\delta^{18}O_{atm}$ changes, we have run 3 different experiments:

– In HSclim we test the impact of the climatic conditions. This simulation is similar to LGM-ctrl, except that the temperature and relative humidity from HS_exp are prescribed as boundary condition.

– In HShydro we test the impact of the hydrological cycle. This simulation is similar to LGM-ctrl, except that $\delta^{18}O_p$ and $\delta^{18}O_{vap}$ from HS_exp are prescribed as boundary condition.

Discussion Paper | Discussion Paper | Discussion Paper | Discussion Paper

CPD

11, 2281–2339, 2015

$\delta^{18}O$ variations during a HS

C. Reutenauer et al.

Title Page

Abstract | Introduction

Conclusions | References

Tables | Figures

|◄ | ►|

◄ | ►

Back | Close

Full Screen / Esc

Printer-friendly Version

Interactive Discussion

– In HSveget we test the impact of the vegetation. This simulation is similar to LGM-ctrl, except that the vegetation production and distribution from HS_exp are prescribed as boundary condition.

Figure 10 summarises the results of the sensitivity analysis in terms of temperature, humidity, oxygen isotopic composition of $\delta^{18}O_p$, $\delta^{18}O_{lw}$, $\delta^{18}O_{lw}$ and $\delta^{18}O_{terr}$. The sensitivity tests show that the implementation of one parameter from HS_exp (HSclim, HShydro and HSveget) leads to a simulated $\delta^{18}O_{terr}$ anomaly similar or higher than in the full HS_exp.

In HSclim, $\delta^{18}O_{terr}$ enrichment is mostly caused by the 0.3 % decrease in relative humidity over the LGM vegetated areas after the AMOC collapse, since $\delta^{18}O_p$ and $\delta^{18}O_{lw}$ are not modified by definition. This global decrease in GPP_O$_2$ weighted relative humidity is not visible in the global HS_exp (Fig. 8) and hence does not explain the $\delta^{18}O_{terr}$ increase in HS_exp. In HSveget, the southward shift of HS_exp vegetation leads to a global GPP_O$_2$ weighted relative humidity decrease by 0.5 %. As in Hsclim, this leads to a high $\delta^{18}O_{terr}$ positive anomaly. The effect of relative humidity on $\delta^{18}O_{terr}$ is minimized in HS_exp, as the southward shift in vegetation counterbalances the change in climatic conditions. This compensation explains why the final GPP_O$_2$ weighted relative humidity does not vary.

In HShydro, the $\delta^{18}O_p$ increase explains the whole $\delta^{18}O_{terr}$ increase. This increase in GPP_O$_2$ weighted $\delta^{18}O_p$ is similar in Hshydro and HS_exp which confirms that the $\delta^{18}O_{terr}$ simulated by the model in the full experiment HS_exp is arising from a change intrinsic to the hydrological cycle, only slightly affected by vegetation distribution.

In addition, note that a weakening of $\delta^{18}O_{lw}$ only occurs with HS vegetation (HS_exp, HSveget), regardless of the climatic conditions. Besides, HSclim depicts a stronger $\delta^{18}O_{lw}$, caused by a higher temperature increase over HS, leading to an enhanced photorespiration fraction among C3 plants. However, the temperature effect on $\delta^{18}O_{lw}$ remains minor.

The global impact of $^{18}\varepsilon_{resp}$ is negligible in all experiments, with variations one order of magnitude lower than $\delta^{18}O_p$.

Finally, sensitivity tests confirm the strong control of hydrological processes on $\delta^{18}O_{terr}$, and highlight the role of the vegetation distribution in defining $\delta^{18}O_p$ and climatic conditions recorded by $\delta^{18}O_{terr}$.

5 Perspective and conclusions

Our study first aimed at testing quantitatively the driving of $\delta^{18}O_{atm}$ by tropical hydrology as suggested by the strong correlation between local records of $\delta^{18}O_c$ and global record of $\delta^{18}O_{atm}$ on the millennial scale. For this we used a HS-type simulation under LGM background conditions with an oxygen isotope mass balance model using spatial and temporal fields of (i) temperature and relative humidity from the AOGCM IPSl-CM4, (ii) PFT distribution and GPP provided by the DVGM ORCHIDEE, (iii) oxygen isotope composition of water vapor and precipitation from the AGCM LMDZ-iso, as well as (iv) the latest isotope fractionation factor measurements involved in respiratory and photosynthetic processes.

Validation of AOGCM outputs feeding the oxygen isotope mass balance model was performed through a model–data comparison of the main drivers of $\delta^{18}O_{terr}$: (i) simulated $\delta^{18}O_p$ was compared to speleothem's calcite $\delta^{18}O$ anomalies, and showed in most sites an excellent agreement despite the complexity of the $\delta^{18}O_c$ signal, (ii) simulated HS humidity to the reconstructed ones, broadly agreeing with paleo-data and (iii) simulated vegetation during LGM and HS, qualitatively consistent with palynological reconstructions.

The model simulates a terrestrial enrichment of $\delta^{18}O_{terr}$ of 0.11‰, which mostly arises from $\delta^{18}O_p$ signal. On a global scale, respiration fractionation only plays a minor role in the anomaly observed during HS, and slightly decreases $\delta^{18}O_{terr}$ in our

δ^{18}O variations during a HS

C. Reutenauer et al.

simulation, driven by a weaker isotope fractionation of soil respiration during HS that masks the effect of increased photorespiration. Results thus confirm the strong control of δ^{18}O$_p$ on δ^{18}O$_{terr}$ at millennial timescale.

The strong control of the low latitude hydrological cycle on simulated δ^{18}O$_{atm}$ on millennial timescales suggests that δ^{18}O$_{atm}$ records at first order changes in monsoonal activity on millennial timescales, in agreement with CH$_4$ mixing ratio variations. Indeed, rapid CH$_4$ variations during the last glacial period are generally attributed to changes in the low latitudes water cycle (Baumgartner et al., 2014; Brook et al., 2000; Chappellaz et al., 1993) driven by latitudinal shifts of the ITCZ and the monsoon systems (e.g. Chiang, 2009). Such signal can also be used for exploring the low latitude hydrological cycle characteristic of Heinrich events. Indeed, Rhodes et al. (2015) recent study suggests that observed CH$_4$ spikes in Wais Divide ice core during the cold phases of HSs represent the hydrological signature of Heinrich Events, through activation of SH wetlands. Guillevic et al. (2014) multi ice-core proxies approach over GS9-HS4 also suggests a decoupling between changes in Greenland temperatures and low latitude hydrology identified in both CH$_4$ and δ^{18}O$_{atm}$, and demonstrates the need for high-resolution data with common precise chronology to explore sub millennial variations.

δ^{18}O$_{atm}$ is a valuated tool to assess the validity of earth system model simulations, as it integrates a combination of hydrological, climatic and biological processes. Besides, δ^{18}O$_{atm}$ is a global signal, which mostly arises from the tropics and integrates all vegetated areas. Therefore, the ability of a model to catch δ^{18}O$_{atm}$ millennial scale variations implies a correct spatial representation of an ensemble of processes. The confrontation of Earth System Models outputs with global proxies such as δ^{18}O$_{atm}$, involving the main components of the climatic system, is crucial to gain confidence in their ability to represent the real world. Our approach is mainly restricted to terrestrial contribution but future modeling exercises should also include the oceanic δ^{18}O$_{atm}$ signal.

References

Ahn, J., Brook, E. J., Schmittner, A., and Kreutz, K.: Abrupt change in atmospheric CO_2 during the last ice age, Geophys. Res. Lett., 39, 18, doi:10.1029/2012GL053018, 2012. 2330

Allison, G., Gat, J., and Leaney, F.: The relationship between deuterium and oxygen-18 delta values in leaf water, Chem. Geol., 58, 145–156, doi:10.1016/0168-9622(85)90035-1, 1985. 2289

Angert, A., Barkan, E., Barnett, B., Brugnoli, E., Davidson, E. A., Fessenden, J., Maneep-ong, S., Panapitukkul, N., Randerson, J. T., Savage, K., Yakir, D., and Luz, B.: Contribution of soil respiration in tropical, temperate, and boreal forests to the [18]O enrichment of atmospheric O_2, Global Biogeochem. Cy., 17, 3, doi:10.1029/2003GB002056, 2003. 2294, 2302

Asmerom, Y., Polyak, V. J., and Burns, S. J.: Variable winter moisture in the southwestern United States linked to rapid glacial climate shifts, Nat. Geosci., 3, 114–117, doi:10.1038/NGEO754, 2010. 2295

Aumont, O. and Bopp, L.: Globalizing results from ocean in situ iron fertilization studies, Global Biogeochem. Cy., 20, 2, doi:10.1029/2005GB002591, 2006. 2304

Badger, M. R., von Caemmerer, S., Ruuska, S., and Nakano, H.: Electron flow to oxygen in higher plants and algae: rates and control of direct photoreduction (Mehler reaction) and rubisco oxygenase, Philos. T. Roy. Soc. B, 355, 1433–1446, doi:10.1098/rstb.2000.0704, 2000. 2294, 2295, 2324

Baker, P., Fritz, S., Burns, S., Ekdahl, E., and Rigsby, C.: The nature and origin of decadal to millennial scale climate variability in the southern tropics of South America: the holocene record of Lago Umayo, Peru, in: Past Climate Variability in South America and Surrounding Regions, edited by: Vimeux, F., Sylvestre, F., and Khodri, M., vol. 14 of Developments in Paleoenvironmental Research, 301–322, Springer, the Netherlands, doi:10.1007/978-90-481-2672-9_13, 2009. 2285

Bariac, T., Rambal, S., Jusserand, C., and Berger, A.: Evaluating water fluxes of field-grown alfalfa from diurnal observations of natural isotope concentrations, energy budget

and ecophysiological parameters, Agr. Forest Meteorol., 48, 263–283, doi:10.1016/0168-1923(89)90073-7, 1989. 2289

Baumgartner, M., Kindler, P., Eicher, O., Floch, G., Schilt, A., Schwander, J., Spahni, R., Capron, E., Chappellaz, J., Leuenberger, M., Fischer, H., and Stocker, T. F.: NGRIP CH_4 concentration from 120 to 10 kyr before present and its relation to a $\delta^{15}N$ temperature reconstruction from the same ice core, Clim. Past, 10, 903–920, doi:10.5194/cp-10-903-2014, 2014. 2307

Bazin, L., Lemieux-Dudon, B., Landais, A., Guillevic, M., Kindler, P., Parrenin, F., and Martinerie, P.: Optimisation of glaciological parameters for ice core chronology by implementing counted layers between identified depth levels, Clim. Past Discuss., 10, 3585–3616, doi:10.5194/cpd-10-3585-2014, 2014. 2282

Bender, M. L.: Orbital tuning chronology for the Vostok climate record supported by trapped gas composition, Earth Planet. Sc. Lett., 204, 275–289, doi:10.1016/S0012-821X(02)00980-9, 2002. 2282

Bender, M. L.,Sowers, T., and Labeyrie, L.: The Dole Effect and its variations during the last 130,000 years as measured in the Vostok Ice Core, Global Biogeochem. Cy., 8, 363–376, doi:10.1029/94GB00724, 1994. 2283, 2284, 2288

Blunier, T., Barnett, B., Bender, M. L., and Hendricks, M. B.: Biological oxygen productivity during the last 60,000 years from triple oxygen isotope measurements, Global Biogeochem. Cy.,16, 3-1–3-13, doi:10.1029/2001GB001460, 2002. 2288

Blunier, T., Bender, M. L., Barnett, B., and von Fischer, J. C.: Planetary fertility during the past 400 ka based on the triple isotope composition of O_2 in trapped gases from the Vostok ice core, Clim. Past, 8, 1509–1526, doi:10.5194/cp-8-1509-2012, 2012. 2283

Bond, G., Broecker, W., Johnsen, S., McManus, J., Labeyrie, L., Jouzel, J., Bonani, G.: Correlations between climate records from North Atlantic sediments and Greenland ice, Nature, 365, 143–147, 1993. 2286

Bopp, L., Kohfeld, K. E., Le Quere, C., and Aumont, O.: Dust impact on marine biota and atmospheric CO_2 during glacial periods, Paleoceanography, 18, 2, doi:10.1029/2002PA000810, 2003. 2304

Broccoli, A. J., Dahl, K. A., and Stouffer, R. J.: Response of the ITCZ to Northern Hemisphere cooling, Geophys. Res. Lett., 33, 1, doi:10.1029/2005GL024546, 2006. 2285

Broecker, W. S.: Abrupt climate change: causal constraints provided by the paleoclimate record, Earth-Sci. Rev., 51, 137–154, 2000. 2286

Back | Close

Full Screen / Esc

Printer-friendly Version

Interactive Discussion

Broecker, W. S., Bond, G., Klas, M., Bonani, G., and Wolfli, W.: A salt oscillator in the glacial Atlantic? 1. The concept, Paleoceanography, 5, 469–477, doi:10.1029/PA005i004p00469, 1990. 2285

Brook, E. J., Harder, S., Severinghaus, J., Steig, E. J., and Sucher, C. M.: On the origin and timing of rapid changes in atmospheric methane during the Last Glacial Period, Global Biogeochem. Cy., 14, 559–572, doi:10.1029/1999GB001182, 2000. 2307

Brook, E. J., White, J. W., Schilla, A. S., Bender, M. L., Barnett, B., Severinghaus, J. P., Taylor, K. C., Alley, R. B., and Steig, E. J.: Timing of millennial-scale climate change at Siple Dome, West Antarctica, during the last glacial period, Quaternary Sci. Rev., 24, 1333–1343, doi:10.1016/j.quascirev.2005.02.002, 2005. 2330

Caley, T., Roche, D. M., Waelbroeck, C., and Michel, E.: Oxygen stable isotopes during the Last Glacial Maximum climate: perspectives from data–model (*i*LOVECLIM) comparison, Clim. Past, 10, 1939–1955, doi:10.5194/cp-10-1939-2014, 2014. 2292

Cappa, C. D., Hendricks, M. B., DePaolo, D. J., and Cohen, R. C.: Isotopic fractionation of water during evaporation, J. Geophys. Res.-Atmos., 108, D16, doi:10.1029/2003JD003597, 2003. 2289

Chappellaz, J., Blunier, T., Raynaud, D., Barnola, J., Schwander, J., and Stauffer, B.: Synchronous changes in atmospheric CH_4 and Greenland Climate between 40-kyr and 8-kyr BP, Nature, 366, 443–445, doi:10.1038/366443a0, 1993. 2307

Chappellaz, J., Stowasser, C., Blunier, T., Baslev-Clausen, D., Brook, E. J., Dallmayr, R., Faïn, X., Lee, J. E., Mitchell, L. E., Pascual, O., Romanini, D., Rosen, J., and Schüpbach, S.: High-resolution glacial and deglacial record of atmospheric methane by continuous-flow and laser spectrometer analysis along the NEEM ice core, Clim. Past, 9, 2579–2593, doi:10.5194/cp-9-2579-2013, 2013. 2286, 2330

Cheng, H., Sinha, A., Wang, X., Cruz, F., and Edwards, R.: The global paleomonsoon as seen through speleothem records from Asia and the Americas, Clim. Dynam., 39, 1045–1062, doi:10.1007/s00382-012-1363-7, 2012. 2286, 2297

Chiang, J. C.: The tropics in paleoclimate, Annu. Rev. Earth Pl. Sc., 37, 263–297, doi:10.1146/annurev.earth.031208.100217, 2009. 2307

Ciais, P., Tagliabue, A., Cuntz, M., Bopp, L., Scholze, M., Hoffmann, G., Lourantou, A., Harrison, S., Prentice, I., Kelley, D., Koven, C. and Piao, S. L.: Large inert carbon pool in the terrestrial biosphere during the Last Glacial Maximum, Nat. Geosci., 5, 74–79, 2012. 2283

Clement, A. C. and Peterson, L. C.: Mechanisms of abrupt climate change of the last glacial period, Rev. Geophys., 46, 4, doi:10.1029/2006RG000204, 2008. 2286

Craig, H. and Gordon, L.: Deuterium and oxygen 18 variations in the ocean and the marine atmosphere, in: Stable Isotopes in Oceanographic Studies and Paleotemperatures, edited by: Tongiorgi, E., 26–30 July 1965, Spoleto, Italy, 1965. 2289

Cvijanovic, I. and Chiang, J.: Global energy budget changes to high latitude North Atlantic cooling and the tropical ITCZ response, Clim. Dynam., 40, 1435–1452, doi:10.1007/s00382-012-1482-1, 2013. 2285

Dahl, K., Broccoli, A., and Stouffer, R.: Assessing the role of North Atlantic freshwater forcing in millennial scale climate variability: a tropical Atlantic perspective, Clim. Dynam., 24, 325–346, doi:10.1007/s00382-004-0499-5, 2005. 2285

Dällenbach, A., Blunier, T., Flückiger, J., Stauffer, B., Chappellaz, J., and Raynaud, D.: Changes in the atmospheric CH_4 gradient between Greenland and Antarctica during the last glacial and the transition to the Holocene, Geophys. Res. Lett., 27, 1005–1008, doi:10.1029/1999GL010873, 2000. 2290

Deplazes, G., Lückge, A., Stuut, J.-B. W., Pätzold, J., Kuhlmann, H., Husson, D., Fant, M., and Haug, G. H.: Weakening and strengthening of the Indian monsoon during Heinrich events and Dansgaard-Oeschger oscillations, Paleoceanography, 29, 99–114, doi:10.1002/2013PA002509, 2014. 2300

Dokken, T. M., Nisancioglu, K. H., Li, C., Battisti, D. S., and Kissel, C.: Dansgaard–Oeschger cycles: interactions between ocean and sea ice intrinsic to the Nordic seas, Paleoceanography, 28, 491–502, doi:10.1002/palo.20042, 2013. 2284

Dongmann, G.: The contribution of land photosynthesis to the stationary enrichment of ^{18}O in the atmosphere, Radiat. Environ. Bioph., 11, 219–225, doi:10.1007/BF01323191, 1974. 2289

Dreyfus, G. B., Parrenin, F., Lemieux-Dudon, B., Durand, G., Masson-Delmotte, V., Jouzel, J., Barnola, J.-M., Panno, L., Spahni, R., Tisserand, A., Siegenthaler, U., and Leuenberger, M.: Anomalous flow below 2700 m in the EPICA Dome C ice core detected using δ^{18}O of atmospheric oxygen measurements, Clim. Past, 3, 341–353, doi:10.5194/cp-3-341-2007, 2007. 2284

Eisenstadt, D., Barkan, E., Luz, B., and Kaplan, A.: Enrichment of oxygen heavy isotopes during photosynthesis in phytoplankton, Photosynth. Res., 103, 97–103, doi:10.1007/s11120-009-9518-z, 2010. 2284, 2288

Elliot, M., Labeyrie, L., and Duplessy, J.-C.: Changes in North Atlantic deep-water formation associated with the Dansgaard-Oeschger temperature oscillations (60–10 ka), Quaternary Sci. Rev., 21, 1153–1165, doi:10.1016/S0277-3791(01)00137-8, 2002. 2285

Farquhar, G. D. and Lloyd, J.: 5 – Carbon and oxygen isotope effects in the exchange of carbon dioxide between terrestrial plants and the atmosphere, in: Stable Isotopes and Plant Carbon-Water Relations, edited by: Farquhar, G. D., Ehleringer, J. R., Hall, A. E., Academic Press, San Diego, 47–70, doi:10.1016/B978-0-08-091801-3.50011-8, 1993. 2291

Farquhar, G. D., von Caemmerer, S., and Berry, J.: A biochemical model of photosynthetic CO_2 assimilation in leaves of C3 species, Planta, 149, 78–90, 1980. 2293

Farquhar, G. D., Hubick, K., Condon, A., and Richards, R.: Carbon isotope fractionation and plant water-use efficiency, in: Stable Isotopes in Ecological Research, Springer, 21–40, 1989. 2290

Farquhar, G. D., Cernusak, L. A., and Barnes, B.: Heavy water fractionation during transpiration, Plant Physiol., 143, 11–18, 2007. 2291

Flanagan, L. B., Bain, J. F., and Ehleringer, J. R.: Stable oxygen and hydrogen isotope composition of leaf water in C3 and C4 plant species under field conditions, Oecologia, 88, 394–400, 1991a. 2290

Flanagan, L. B., Comstock, J. P., and Ehleringer, J. R.: Comparison of modeled and observed environmental influences on the stable oxygen and hydrogen isotope composition of leaf water in Phaseolus vulgaris L., Plant Physiol., 96, 588–596, 1991b. 2289

Flanagan, L. B., Marshall, J. D., and Ehleringer, J. R.: Photosynthetic gas exchange and the stable isotope composition of leaf water: comparison of a xylem-tapping mistletoe and its host, Plant Cell Environ., 16, 623–631, doi:10.1111/j.1365-3040.1993.tb00480.x, 1993. 2290

Flanagan, L. B., Phillips, S. L., Ehleringer, J. R., Lloyd, J., and Farquhar, G. D.: Effect of changes in leaf water oxygen isotopic composition on discrimination against $C^{18}O^{16}O$ during photosynthetic gas exchange, Funct. Plant Biol., 21, 221–234, 1994. 2290

Fleitmann, D., Cheng, H., Badertscher, S., Edwards, R. L., Mudelsee, M., Gktürk, O. M., Fankhauser, A., Pickering, R., Raible, C. C., Matter, A., Kramers, J., and Tüysüz, O.: Timing and climatic impact of Greenland interstadials recorded in stalagmites from northern Turkey, Geophys. Res. Lett., 36, 19, doi:10.1029/2009GL040050, 2009. 2286, 2295

Fletcher, W. J., Goni, M. F. S., Allen, J. R., Cheddadi, R., Combourieu-Nebout, N., Huntley, B., Lawson, I., Londeix, L., Magri, D., Margari, V., Müller, U. C., Naughton, F., Novenko, E., Roucoux, K., and Tzedakis, P.: Millennial-scale variability during the

last glacial in vegetation records from Europe, Quaternary Sci. Rev., 29, 2839–2864, doi:10.1016/j.quascirev.2009.11.015, 2010. 2299

Flückiger, J., Dällenbach, A., Blunier, T., Stauffer, B., Stocker, T. F., Raynaud, D., and Barnola, J.-M.: Variations in atmospheric N_2O concentration during abrupt climatic changes, Science, 285, 227–230, doi:10.1126/science.285.5425.227, 1999. 2290

Genty, D., Blamart, D., Ouahdi, R., Gilmour, M., Baker, A., Jouzel, J., and Van-Exter, S.: Precise dating of Dansgaard–Oeschger climate oscillations in western Europe from stalagmite data, Nature, 421, 833–837, 2003. 2295

Gillon, J. and Yakir, D.: Influence of carbonic anhydrase activity in terrestrial vegetation on the ^{18}O content of atmospheric CO_2, Science, 291, 2584–2587, doi:10.1126/science.1056374, 2001. 2324

Grootes, P. M. and Stuiver, M.: Oxygen 18/16 variability in Greenland snow and ice with 10^3 to 10^5 year time resolution, J. Geophys. Res.-Oceans, 102, 26455–26470, doi:10.1029/97JC00880, 1997. 2295

Grousset, F., Labeyrie, L., Sinko, J., Cremer, M., Bond, G., Duprat, J., Cortijo, E., and Huon, S.: Patterns of ice-rafted detritus in the glacial North Atlantic (40–55 N), Paleoceanography, 8, 175–192, 1993. 2285

Guillevic, M.: Characterisation of rapid climate changes through isotope analyses of ice and entrapped air in the NEEM ice core, PhD thesis, Versailles-St Quentin en Yvelines, 2013. 2330

Guillevic, M., Bazin, L., Landais, A., Stowasser, C., Masson-Delmotte, V., Blunier, T., Eynaud, F., Falourd, S., Michel, E., Minster, B., Popp, T., Prié, F., and Vinther, B. M.: Evidence for a three-phase sequence during Heinrich Stadial 4 using a multiproxy approach based on Greenland ice core records, Clim. Past, 10, 2115–2133, doi:10.5194/cp-10-2115-2014, 2014. 2285, 2286, 2301, 2307, 2330

Guy, R. D., Fogel, M. L., and Berry, J. A.: Photosynthetic Fractionation of the Stable Isotopes of Oxygen and Carbon, Plant Physiol., 101, 37–47, doi:10.1104/pp.101.1.37, 1993. 2288

Handiani, D., Paul, A., and Dupont, L.: Tropical climate and vegetation changes during Heinrich Event 1: a model–data comparison, Clim. Past, 8, 37–57, doi:10.5194/cp-8-37-2012, 2012. 2299, 2329

Harrison, S. and Goni, M. S.: Global patterns of vegetation response to millennial-scale variability and rapid climate change during the last glacial period, Quaternary Sci. Rev., 29, 2957–2980, doi:10.1016/j.quascirev.2010.07.016, 2010. 2299

$\delta^{18}O$ variations during a HS

C. Reutenauer et al.

Title Page

Abstract	Introduction
Conclusions	References
Tables	Figures

◄ | ►►

◄ | ►

Back | Close

Full Screen / Esc

Printer-friendly Version

Interactive Discussion

Heinrich, H.: Origin and consequences of cyclic ice rafting in the northeast Atlantic Ocean during the past 130,000 years, Quaternary Res., 29, 142–152, 1988. 2285

Helman, Y., Barkan, E., Eisenstadt, D., Luz, B., and Kaplan, A.: Fractionation of the three stable oxygen isotopes by oxygen-producing and oxygen-consuming reactions in photosynthetic organisms, Plant Physiol., 138, 2292–2298, doi:10.1104/pp.105.063768, 2005. 2283, 2324

Hendricks, M. B., Bender, M. L., and Barnett, B. A.: Net and gross O_2 production in the southern ocean from measurements of biological O_2 saturation and its triple isotope composition, Deep-Sea Res. Pt. I, 51, 1541–1561, doi:10.1016/j.dsr.2004.06.006, 2004. 2284, 2288

Hessler, I., Dupont, L., Bonnefille, R., Behling, H., Gonzalez, C., Helmens, K. F., Hooghiemstra, H., Lebamba, J., Ledru, M.-P., Lezine, A.-M., Maley, J., Marret, F., and Vincens, A.: Millennial-scale changes in vegetation records from tropical Africa and South America during the last glacial, Quaternary Sci. Rev., 29, 2882–2899, doi:10.1016/j.quascirev.2009.11.029, 2010. 2299

Hoffmann, G., Cuntz, M., Weber, C., Ciais, P., Friedlingstein, P., Heimann, M., Jouzel, J., Kaduk, J., Maier-Reimer, E., Seibt, U., and Six, K.: A model of the Earth's Dole effect, Global Biogeochem. Cy., 18, 1, doi:10.1029/2003GB002059, 2004. 2283, 2287, 2288, 2293, 2294, 2302

Huber, C., Leuenberger, M., Spahni, R., Flückiger, J., Schwander, J., Stocker, T., Johnsen, S., Landais, A., and Jouzel, J.: Isotope calibrated Greenland temperature record over marine isotope stage 3 and its relation to CH_4, Earth Planet. Sc. Lett., 243, 504–519, 2006. 2284

Jimenez-Moreno, G., Anderson, R. S., Desprat, S., Grigg, L. D., Grimm, E. C., Heusser, L. E., Jacobs, B. F., Lopez-Martinez, C., Whitlock, C. L., and Willard, D. A.: Millennial-scale variability during the last glacial in vegetation records from North America, Quaternary Sci. Rev., 29, 2865–2881, doi:10.1016/j.quascirev.2009.12.013, 2010. 2299

Kageyama, M., Mignot, J., Swingedouw, D., Marzin, C., Alkama, R., and Marti, O.: Glacial climate sensitivity to different states of the Atlantic meridional overturning circulation: results from the IPSL model, Clim. Past, 5, 551–570, doi:10.5194/cp-5-551-2009, 2009. 2290, 2291, 2295, 2300

Kageyama, M., Paul, A., Roche, D. M., and Meerbeeck, C. J. V.: Modelling glacial climatic millennial-scale variability related to changes in the Atlantic meridional overturning circulation: a review, Quaternary Sci. Rev., 29, 2931–2956, doi:10.1016/j.quascirev.2010.05.029, 2010. 2285

Title Page

Abstract | Introduction

Conclusions | References

Tables | Figures

◄◄ | ►►

◄ | ►

Back | Close

Full Screen / Esc

Printer-friendly Version

Interactive Discussion

Kageyama, M., Merkel, U., Otto-Bliesner, B., Prange, M., Abe-Ouchi, A., Lohmann, G., Ohgaito, R., Roche, D. M., Singarayer, J., Swingedouw, D., and X Zhang: Climatic impacts of fresh water hosing under Last Glacial Maximum conditions: a multi-model study, Clim. Past, 9, 935–953, doi:10.5194/cp-9-935-2013, 2013. 2284, 2285, 2291

Kanner, L. C., Burns, S. J., Cheng, H., and Edwards, R. L.: High-latitude forcing of the South American summer monsoon during the last glacial, Science, 335, 570–573, doi:10.1126/science.1213397, 2012. 2295

Kanner, L. C., Buenning, N. H., Stott, L. D., Timmermann, A., and Noone, D.: The role of soil processes in [18]O terrestrial climate proxies, Global Biogeochem. Cy., 28, 239–252, doi:10.1002/2013GB004742, 2014. 2292

Kawamura, K., Parrenin, F., Lisiecki, L., Uemura, R., Vimeux, F., Severinghaus, J. P., Hutterli, M. A., Nakazawa, T., Aoki, S., Jouzel, J., Raymo, M. E., Matsumoto, K., Nakata, H., Motoyama, H., Fujita, S., Goto-Azuma, K., Fujii, Y., and Watanabe, O.: Northern hemisphere forcing of climatic cycles in Antarctica over the past 360,000 years, Nature, 448, 912–U4, doi:10.1038/nature06015, 2007. 2282

Keeling, R. F.: Development of an interferometric oxygen analyzer for precise measurement of the atmospheric O_2 mole fraction, PhD thesis, Harvard University, 1988. 2293

Kindler, P., Guillevic, M., Baumgartner, M., Schwander, J., Landais, A., and Leuenberger, M.: Temperature reconstruction from 10 to 120 kyr b2k from the NGRIP ice core, Clim. Past, 10, 887–902, doi:10.5194/cp-10-887-2014, 2014. 2284

Kleppin, H., Jochum, M., Otto-Bliesner, B., Shields, C. A., and Yeager, S.: Stochastic atmospheric forcing as trigger for sudden Greenland warmings, J. Climate, in review, 2015. 2284

Kohfeld, K. E., Quere, C. L., Harrison, S. P., and Anderson, R. F.: Role of marine biology in glacial-interglacial CO_2 cycles, Science, 308, 74–78, doi:10.1126/science.1105375, 2005. 2304

Krebs, U. and Timmermann, A.: Tropical air-sea interactions accelerate the recovery of the Atlantic meridional overturning circulation after a major shutdown, J. Climate, 20, 4940–4956, 2007. 2285

Krinner, G., Viovy, N., de Noblet-Ducoudre, N., Ogee, J., Polcher, J., Friedlingstein, P., Ciais, P., Sitch, S., and Prentice, I. C.: A dynamic global vegetation model for studies of the coupled atmosphere-biosphere system, Global Biogeochem. Cy., 19, 1, doi:10.1029/2003GB002199, 2005. 2292

Landais, A., Barnola, J. M., Masson-Delmotte, V., Jouzel, J., Chappellaz, J., Caillon, N., Huber, C., Leuenberger, M., and Johnsen, S. J.: A continuous record of temperature evolution over a sequence of Dansgaard-Oeschger events during Marine Isotopic Stage 4 (76 to 62 kyr BP), Geophys. Res. Lett., 31, 22 doi:10.1029/2004GL021193, 2004. 2284

5 Landais, A., Lathiere, J., Barkan, E., and Luz, B.: Reconsidering the change in global biosphere productivity between the Last Glacial Maximum and present day from the triple oxygen isotopic composition of air trapped in ice cores, Global Biogeochem. Cy., 21, 1, doi:10.1029/2006GB002739, 2007a. 2288, 2295

Landais, A., Masson-Delmotte, V., Nebout, N. C., Jouzel, J., Blunier, T., Leuenberger, M.,
10 Dahl-Jensen, D., and Johnsen, S.: Millenial scale variations of the isotopic composition of atmospheric oxygen over marine isotopic stage 4, Earth Planet. Sc. Lett., 258, 101–113, doi:10.1016/j.epsl.2007.03.027, 2007b. 2284, 2286, 2287, 2324

Landais, A., Dreyfus, G., Capron, E., Masson-Delmotte, V., Sanchez-Goñi, M. F., Desprat, S., Hoffmann, G., Jouzel, J., Leuenberger, M., and Johnsen, S.: What drives
15 the millennial and orbital variations of $\delta^{18}O_{atm}$?, Quaternary Sci. Rev., 29, 235–246, doi:10.1016/j.quascirev.2009.07.005, 2010. 2283, 2286, 2287

Landais, A., Dreyfus, G., Capron, E., Pol, K., Loutre, M. F., Raynaud, D., Lipenkov, V. Y., Arnaud, L., Masson-Delmotte, V., Paillard, D., Jouzel, J., and Leuenberger, M.: Towards orbital dating of the EPICA Dome C ice core using $\delta O_2/N_2$, Clim. Past, 8, 191–203, doi:10.5194/cp-
20 8-191-2012, 2012. 2282

Lewis, S. C., LeGrande, A. N., Kelley, M., and Schmidt, G. A.: Water vapour source impacts on oxygen isotope variability in tropical precipitation during Heinrich events, Clim. Past, 6, 325–343, doi:10.5194/cp-6-325-2010, 2010. 2296, 2325

Li, C., Battisti, D. S., Schrag, D. P., and Tziperman, E.: Abrupt climate shifts in Green-
25 land due to displacements of the sea ice edge, Geophys. Res. Lett., 32, L19702, 19, 10.1029/2005GL023492, 2005. 2284

Li, C., Battisti, D. S., and Bitz, C. M.: Can North Atlantic sea ice anomalies account for Dansgaard–Oeschger climate signals?, J. Climate, 23, 5457-5475,10.1175/2010JCLI3409.1, 2010. 2284

30 Liu, Z., Otto-Bliesner, B. L., He, F., Brady, E. C., Tomas, R., Clark, P. U., Carlson, A. E., Lynch-Stieglitz, J., Curry, W., Brook, E., Erickson, D., Jacob, R., Kutzbach, J., and Cheng, J.: Transient Simulation of Last Deglaciation with a New Mechanism for Bølling-Allerød Warming, Science, 325, 310–314, doi:10.1126/science.1171041, 2009. 2285

Title Page

Abstract | Introduction

Conclusions | References

Tables | Figures

◄ | ►

◄ | ►

Back | Close

Full Screen / Esc

Printer-friendly Version

Interactive Discussion

Lloyd, J. and Farquhar, G.: ^{13}C discrimination during CO_2 assimilation by the terrestrial biosphere, Oecologia, 99, 201–215, doi:10.1007/BF00627732, 1994. 2291

Luz, B. and Barkan, E.: Proper estimation of marine gross O_2 production with $^{17}O/^{16}O$ and $^{18}O/^{16}O$ ratios of dissolved O_2, Geophys. Res. Lett., 38, 19, 10.1029/2011GL049138, 2011a. 2288

Luz, B. and Barkan, E.: The isotopic composition of atmospheric oxygen, Global Biogeochem. Cy., 25, 3, doi:10.1029/2010GB003883, 2011b. 2284

Luz, B., Barkan, E., Bender, M., Thiemens, M., and Boering, K.: Triple-isotope composition of atmospheric oxygen as a tracer of biosphere productivity, Nature, 400, 547–550, doi:10.1038/22987, 1999. 2283

Luz, B., Barkan, E., Yam, R., and Shemesh, A.: Fractionation of oxygen and hydrogen isotopes in evaporating water, Geochim. Cosmochim. Ac., 73, 6697–6703, doi:10.1016/j.gca.2009.08.008, 2009. 2289

Luz, B., Barkan, E., and Severinghaus, J.: 5.14 – The stable isotopic composition of atmospheric O_2, in: Treatise on Geochemistry, edited by: Holland, H. D. and Turekian, K. K., Elsevier, Oxford, 2nd edn., 363–383, doi:10.1016/B978-0-08-095975-7.00419-8, 2014. 2288, 2301, 2303, 2324

Majoube, M.: Fractionnement en oxygene-18 et en deuterium entre l'eau et sa vapeur, J. Chim. Phys, 68, 1423–1436, 1971. 2289

Mariotti, V., Bopp, L., Tagliabue, A., Kageyama, M., and Swingedouw, D.: Marine productivity response to Heinrich events: a model–data comparison, Clim. Past, 8, 1581–1598, doi:10.5194/cp-8-1581-2012, 2012. 2304

Marti, O., Braconnot, P., Dufresne, J.-L., Bellier, J., Benshila, R., Bony, S., Brockmann, P., Cadule, P., Caubel, A., Codron, F., de Noblet, N., Denvil, S., Fairhead, L., Fichefet, T., Foujols, M.-A., Friedlingstein, P., Goosse, H., Grandpeix, J.-Y., Guilyardi, E., Hourdin, F., Idelkadi, A., Kageyama, M., Krinner, G., Lžvy, C, Madec, G., Mignot, J., Musat, I., Swingedouw, D. and Talandier, C.: Key features of the IPSL ocean atmosphere model and its sensitivity to atmospheric resolution, Clim. Dynam., 34, 1–26, 2010. 2290

McGuire, K., DeWalle, D., and Gburek, W.: Evaluation of mean residence time in subsurface waters using oxygen-18 fluctuations during drought conditions in the mid-Appalachians, J. Hydrol., 261, 132–149, doi:10.1016/S0022-1694(02)00006-9, 2002. 2292

Discussion Paper | Discussion Paper | Discussion Paper | Discussion Paper |

CPD

11, 2281–2339, 2015

$\delta^{18}O$ variations during a HS

C. Reutenauer et al.

Title Page

Abstract | Introduction

Conclusions | References

Tables | Figures

◄ | ►

◄ | ►

Back | Close

Full Screen / Esc

Printer-friendly Version

Interactive Discussion

Menviel, L., Timmermann, A., Mouchet, A., and Timm, O.: Meridional reorganizations of marine and terrestrial productivity during Heinrich events, Paleoceanography, 23, 1, doi:10.1029/2007PA001445, 2008. 2304

Menviel, L., Timmermann, A., Friedrich, T., and England, M. H.: Hindcasting the continuum of Dansgaard–Oeschger variability: mechanisms, patterns and timing, Clim. Past, 10, 63–77, doi:10.5194/cp-10-63-2014, 2014. 2285

Merlivat, L.: Molecular diffusivities of $H_2^{16}O, HD^{16}O$, and $H_2^{18}O$ in gases, J. Chem. Phys., 69, 2864–2871, doi:10.1063/1.436884, 1978. 2289, 2290

Mohtadi, M., Oppo, D. W., Steinke, S., Stuut, J.-B. W., De Pol-Holz, R., Hebbeln, D., and Lückge, A.: Glacial to Holocene swings of the Australian-Indonesian monsoon, Nat. Geosci., 4, 540–544, 2011. 2295

Monnin, E., Indermühle, A., Dällenbach, A., Flückiger, J., Stauffer, B., Stocker, T. F., Raynaud, D., and Barnola, J.-M.: Atmospheric CO_2 Concentrations over the Last Glacial Termination, Science, 291, 112–114, doi:10.1126/science.291.5501.112, 2001. 2290

NGRIP members, Andersen, K., Azuma, N., Barnola, J., Bigler, M., Biscaye, P., Caillon, N., Chappellaz, J., Clausen, H., DahlJensen, D., Fischer, H., Fluckiger, J., Fritzsche, D., Fujii, Y., Goto-Azuma, K., Gronvold, K., Gundestrup, N., Hansson, M., Huber, C., Hvidberg, C., Johnsen, S., Jonsell, U., Jouzel, J., Kipfstuhl, S., Landais, A., Leuenberger, M., Lorrain, R., Masson-Delmotte, V., Miller, H., Motoyama, H., Narita, H., Popp, T., Rasmussen, S., Raynaud, D., Rothlisberger, R., Ruth, U., Samyn, D., Schwander, J., Shoji, H., Siggard-Andersen, M., Steffensen, J., Stocker, T., Sveinbjornsdottir, A., Svensson, A., Takata, M., Tison, J., Thorsteinsson, T., Watanabe, O., Wilhelms, F., White, J. W. C.: High-resolution record of Northern Hemisphere climate extending into the last interglacial period, Nature, 431, 147–151, doi:10.1038/nature02805, 2004. 2284

Otto-Bliesner, B. L. and Brady, E. C.: The sensitivity of the climate response to the magnitude and location of freshwater forcing: last glacial maximum experiments, Quaternary Sci. Rev., 29, 56–73, doi:10.1016/j.quascirev.2009.07.004, 2010. 2285

Pausata, F. S., Battisti, D. S., Nisancioglu, K. H., and Bitz, C. M.: Chinese stalagmite [delta] ^{18}O controlled by changes in the Indian monsoon during a simulated Heinrich event, Nat. Geosci., 4, 474–480, 2011. 2286, 2296, 2325, 2333

Peltier, W.: Global glacial isostasy and the surface of the ice-age Earth: the ICE-5G (VM2) model and GRACE, Annu. Rev. Earth Pl. Sc., 32, 111–149, 2004. 2290

Discussion Paper | Discussion Paper | Discussion Paper | Discussion Paper |

CPD

11, 2281–2339, 2015

$\delta^{18}O$ variations during a HS

C. Reutenauer et al.

Title Page

Abstract   Introduction

Conclusions   References

Tables   Figures

◄◄   ►►

◄   ►

Back   Close

Full Screen / Esc

Printer-friendly Version

Interactive Discussion

Peterson, L. C. and Haug, G. H.: Variability in the mean latitude of the Atlantic intertropical convergence zone as recorded by riverine input of sediments to the Cariaco Basin (Venezuela), Palaeogeogr. Palaeocl., 234, 97–113, doi:10.1016/j.palaeo.2005.10.021, 2006. 2295

Prentice, I. C., Jolly, D., and Afanaseva, N. B., Ager, T. A., Anderson, K., Anderson, P. M., Andrieu, V., Andreev, A. A., Ballouche, A., Bartlein, P. J., de Beaulieu, J. L., Bengo, M., Berezina, N. A., Bezusko, L. G., Bezusko, T. V., Bigelow, N. H., Blyakharchuk, T. A., Bolikhovskaya, N. S., Bonnefille, R., Bottema, S., Bržnac, P., Brubaker, L. B., Buchet, G., Burney, D., Bykova, G. V., Cheddadi, R., Chen, X., Chernavskaya, M. M., Chernova, G. M., Cwynar, L. C., Dorofeyuk, N. I., Dirksen, V. G., Edorh, T., Edwards, M. E., Eisner, W. R., Elenga, H., Elina, G. A., Elmoutaki, S., Filimonova, L. V., Glebov, F. Z., Guiot, J., Gunova, V. S., Hamilton, A. C., Han, H., Harrison, S. P., Hu, F.-S., Huang, C., Huntley, B., Jolly, D., Jonson, H., Ke, M., Khomutova, V. I., Kong Z., Kvavadze, E. V., Laarif, F., Lamb, H. E., Lžzine, A.-M., Li, S., Li, W., Liew, P., Liu, G., Liu, J., Liu, Q., Liu, K.-B., Lozhkin, A. V., Maley, J., Marchant, R., Mbenza, M., MacDonald, G. M., Miyoshi, N., Mock, C. J., Morita, Y., Newby, P.,Ni, J., Osipova, I. R., Panova, N. K., Perez-Obiol, R., Peyron, O., Prentice, I. C., Qiu, W., Reille, M., Ren, G., Reynaud-Farrera, I., Richard, P. J. H., Riollet, G., Ritchie, J. C., Roche, E., Saarse, L., Scott, L., Sevastyanov, D. V., Sher, A. V., Song, C., Spear, R. W., Ssemmanda, I., Straka, H., Sugita, S., Sun, X., Takahara, H., Tang, L., Tarasov, P. E., Taylor, D., Thompson, R. S., Uchiyama, T., Van Campo, E., Vilimumbalo, S., Vincens, A., Volkova, V. S., Waller, M., Webb, T., Williams, J. W., Xia, Y., Xu, Q., Yan, S., Yang, X., Yu, G., Zernitskaya, V. P., Zhao, J., Zheng, Z.: Mid-Holocene and glacial-maximum vegetation geography of the northern continents and Africa, J. Biogeogr., 27, 507–519, 2000. 2298

Raich, J. W. and Potter, C. S.: Global patterns of carbon dioxide emissions from soils, Global Biogeochem. Cy., 9, 23–36, doi:10.1029/94GB02723, 1995. 2294, 2302

Rasmussen, S. O., Abbott, P. M., Blunier, T., Bourne, A. J., Brook, E., Buchardt, S. L., Buizert, C., Chappellaz, J., Clausen, H. B., Cook, E., Dahl-Jensen, D., Davies, S. M., Guillevic, M., Kipfstuhl, S., Laepple, T., Seierstad, I. K., Severinghaus, J. P., Steffensen, J. P., Stowasser, C., Svensson, A., Vallelonga, P., Vinther, B. M., Wilhelms, F., and Winstrup, M.: A first chronology for the North Greenland Eemian Ice Drilling (NEEM) ice core, Clim. Past, 9, 2713–2730, doi:10.5194/cp-9-2713-2013, 2013. 2286, 2330

Rhodes, R. H., Brook, E. J., Chiang, J. C. H., Blunier, T., Maselli, O. J., McConnell, J. R., Romanini, D., and Severinghaus, J. P.: Enhanced tropical methane pro-

Title Page

Abstract | Introduction

Conclusions | References

Tables | Figures

|◄ | ►|

◄ | ►

Back | Close

Full Screen / Esc

Printer-friendly Version

Interactive Discussion

duction in response to iceberg discharge in the North Atlantic, Science, 348, 1016–1019, doi:10.1126/science.1262005, 2015. 2307

Risi, C., Bony, S., Vimeux, F., and Jouzel, J.: Water-stable isotopes in the LMDZ4 general circulation model: model evaluation for present-day and past climates and applications to climatic interpretations of tropical isotopic records, J. Geophys. Res.-Atmos., 115, D12, doi:10.1029/2009JD013255, 2010. 2291, 2292

Roche, D., Wiersma, A., and Renssen, H.: A systematic study of the impact of freshwater pulses with respect to different geographical locations, Clim. Dynam., 34, 997–1013, doi:10.1007/s00382-009-0578-8, 2010. 2285

Ruddiman, W. F.: Late Quaternary deposition of ice-rafted sand in the subpolar North Atlantic (lat 40 to 65 N), Geol. Soc. Am. Bull., 88, 1813–1827, 1977. 2285

Sanchez Goni, M. F. and Harrison, S. P.: Millennial-scale climate variability and vegetation changes during the last glacial: concepts and terminology, Quaternary Sci. Rev., 29, 2823–2827, doi:10.1016/j.quascirev.2009.11.014, 2010. 2285

Schlesinger, W. and Andrews, J.: Soil respiration and the global carbon cycle, Biogeochemistry, 48, 7–20, doi:10.1023/A:1006247623877, 2000. 2302, 2324

Schmittner, A.: Decline of the marine ecosystem caused by a reduction in the Atlantic overturning circulation, Nature, 434, 628–633, doi:10.1038/nature03476, 2005. 2304

Schmittner, A. and Galbraith, E. D.: Glacial greenhouse-gas fluctuations controlled by ocean circulation changes, Nature, 456, 373–376, 2008. 2304

Severinghaus, J. P.: Studies of the terrestrial O_2 and carbon cycles in sand dune gases and in biosphere 2, Tech. rep., Oak Ridge Associated Universities, Inc., TN, 1995. 2293

Severinghaus, J. P., Beaudette, R., Headly, M. A., Taylor, K., and Brook, E. J.: Oxygen-18 of O_2 records the impact of abrupt climate change on the terrestrial biosphere, Science, 324, 1431–1434, doi:10.1126/science.1169473, 2009. 2284, 2286, 2287, 2288, 2301, 2331

Stouffer, R. J., Yin, J., Gregory, J., Dixon, K., Spelman, M., Hurlin, W., Weaver, A., Eby, M., Flato, G., Hasumi, H., Hu, A., Jungclaus, J. H., Kamenkovich, I. V., Levermann, A., Montoya, M., Murakami, S., Nawrath, S., Oka, A., Peltier, W. R., Robitaille, D. Y. , Sokolov, A., Vettoretti, G. and Weber, S. L.: Investigating the causes of the response of the thermohaline circulation to past and future climate changes, J. Climate, 19, 1365–1387, 10.1175/JCLI3689.1, 2006. 2284

Swingedouw, D., Mignot, J., Braconnot, P., Mosquet, E., Kageyama, M., and Alkama, R.: Impact of freshwater release in the North Atlantic under different climate conditions in an OAGCM, J. Climate, 22, 6377–6403, 2009. 2285

Tagliabue, A., Bopp, L., and Aumont, O.: Evaluating the importance of atmospheric and sedimentary iron sources to Southern Ocean biogeochemistry, Geophys. Res. Lett., 36, 13, doi:10.1029/2009GL038914, 2009. 2304

Takahara, H., Igarashi, Y., Hayashi, R., Kumon, F., Liew, P.-M., Yamamoto, M., Kawai, S., Oba, T., and Irino, T.: Millennial-scale variability in vegetation records from the East Asian islands: Taiwan, Japan and Sakhalin, Quaternary Sci. Rev., 29, 2900–2917, doi:10.1016/j.quascirev.2009.11.026, 2010. 2299

Von Caemmerer, S.: Biochemical Models of Leaf Photosynthesis, 2, Csiro publishing, 2000. 2294, 2302

Waelbroeck, C., Labeyrie, L., Michel, E., Duplessy, J., McManus, J., Lambeck, K., Balbon, E., and Labracherie, M.: Sea-level and deep water temperature changes derived from benthic foraminifera isotopic records, Quaternary Sci. Rev., 21, 295–305, doi:10.1016/S0277-3791(01)00101-9, 2002. 2303, 2324

Walker, C. D. and Brunel, J.-P.: Examining evapotranspiration in a semi-arid region using stable isotopes of hydrogen and oxygen, J. Hydrol., 118, 55–75, doi:10.1016/0022-1694(90)90250-2, 1990. 2289

Walker, C. D., Leaney, F. W., Dighton, J. C., and Allison, G. B.: The influence of transpiration on the equilibration of leaf water with atmospheric water vapour, Plant Cell Environ., 12, 221–234, doi:10.1111/j.1365-3040.1989.tb01937.x, 1989. 2289

Wang, L., Good, S. P., Caylor, K. K., and Cernusak, L. A.: Direct quantification of leaf transpiration isotopic composition, Agr. Forest Meteorol., 154–155, 127–135, doi:10.1016/j.agrformet.2011.10.018, 2012. 2292

Wang, Y. J., Cheng, H., Edwards, R. L., He, Y., Kong, X., An, Z., Wu, J., Kelly, M. J., Dykoski, C. A., and Li, X.: The holocene asian monsoon: links to solar changes and North Atlantic climate, Science, 308, 854–857, doi:10.1126/science.1106296, 2005. 2333

Wang, Y. J., Cheng, H., Edwards, R. L., Kong, X., Shao, X., Chen, S., Wu, J., Jiang, X., Wang, X., and An, Z.: Millennial- and orbital-scale changes in the East Asian monsoon over the past 224,000 years, Nature, 451, 1090–1093, doi:10.1038/nature06692, 2008. 2284, 2286, 2295

Title Page

Abstract | Introduction

Conclusions | References

Tables | Figures

◄◄ | ►►

◄ | ►

Back | Close

Full Screen / Esc

Printer-friendly Version

Interactive Discussion

Wang, Y. J., Cheng, H., Edwards, R. L., An, Z. S., Wu, J. Y., Shen, C.-C., and Dorale, J. A.: A high-resolution absolute-dated late pleistocene monsoon record from Hulu Cave, China, Science, 294, 2345–2348, doi:10.1126/science.1064618, 2001. 2286, 2295

Weldeab, S.: Bipolar modulation of millennial-scale West African monsoon variability during the last glacial (75,000–25,000 years ago), Quaternary Sci. Rev., 40, 21–29, doi:10.1016/j.quascirev.2012.02.014, 2012. 2295

Woillez, M.-N.: Modellisation des variations rapides du systeme atmospherere-ocean-vegetation-cryosphere en climats glaciaires, PhD thesis, Paris Versailles St-Quentin, 2012. 2293

Woillez, M.-N., Kageyama, M., Krinner, G., de Noblet-Ducoudré, N., Viovy, N., and Mancip, M.: Impact of CO_2 and climate on the Last Glacial Maximum vegetation: results from the ORCHIDEE/IPSL models, Clim. Past, 7, 557–577, doi:10.5194/cp-7-557-2011, 2011. 2293, 2298, 2300

Woillez, M.-N., Kageyama, M., Combourieu-Nebout, N., and Krinner, G.: Simulating the vegetation response in western Europe to abrupt climate changes under glacial background conditions, Biogeosciences, 10, 1561–1582, doi:10.5194/bg-10-1561-2013, 2013. 2291, 2293, 2295, 2299, 2300

Yakir, D., D., DeNiro, M. J., and Gat, J. R.: Natural deuterium and oxygen-18 enrichment in leaf water of cotton plants grown under wet and dry conditions: evidence for water compartmentation and its dynamics, Plant Cell Environ., 13, 49–56, doi:10.1111/j.1365-3040.1990.tb01298.x, 1990. 2289

Title Page

Abstract | Introduction

Conclusions | References

Tables | Figures

◄ | ►

◄ | ►

Back | Close

Full Screen / Esc

Printer-friendly Version

Interactive Discussion

Table 1. Plant functional types (PFT) in ORCHIDEE, acronyms used and mega-biome assignment in this study.

PFT	Acronym	Mega-biome
Bare soil	Bare soil	Bare soil
Tropical broadleaf evergreen trees	TrBE	Tropical trees
Tropical broadleaf raingreen trees	TrBR	Tropical trees
Temperate needleleaf evergreen trees	TempNE	Temperate trees
Temperate broadleaf evergreen trees	TempBE	Temperate trees
Temperate broadleaf summergreen trees	TempBS	Temperate trees
Boreal needleleaf evergreen trees	BoNE	Boreal trees
Boreal broadleaf summergreen trees	BoBS	Boreal trees
Boreal needleleaf summergreen trees	BoNS	Boreal trees
C3 grass	C3 grass	C3 grass
C4 grass	C4 grass	C4 grass

Discussion Paper | Discussion Paper | Discussion Paper | Discussion Paper

CPD

11, 2281–2339, 2015

δ^{18}O variations during a HS

C. Reutenauer et al.

Title Page

Abstract | Introduction

Conclusions | References

Tables | Figures

|◄ | ►|

◄ | ►

Back | Close

Full Screen / Esc

Printer-friendly Version

Interactive Discussion

Table 2. Parameters involved in the calculation of δ^{18}O$_{\text{atm}}$. Uncertainties are given for most of the parameters except for those derived from the ORCHIDEE model.

Parameter	Unit	Definition	LGM_ctrl	HS_exp
$[CO_2]$	ppm	carbon dioxide mixing ratio in the troposphere	190	190
t	°C	temperature at the site of photosynthesis	21.08	21.41
h	%	relative humidity at the site of photosynthesis	66.09	66.12
GPP_C	Pmol C yr^{-1}	gross photosynthetic molar carbon flux from the terrestrial biosphere	6.758	6.450
GPP_O$_2$	Pmol O$_2$ yr^{-1}	gross Photosynthetic molar oxygen flux from the terrestrial biosphere	11.768	11.410
f_{C4}	%	C4 fraction (in terms of GPP_C)	36.92	35.59
f_{photo}	%	fraction of photorespiration	28.55	29.52
f_{soil_dark}	%	soil fraction of dark respiration	62[a]	62[a]
f_{dark_soil}	%	fraction of soil respiration	38.10	37.50
f_{dark_leaves}	%	fraction of leaf respiration	23.35	22.98
f_{Mehler}	%	fraction of Mehler respiration	10[b]	10[b]
$^{18}\varepsilon_{dark\_soil}$	‰	global isotopic fractionation associated with dark soil respiration	15.895 ± 0.5[c]	15.610 ± 0.5[c]
$^{18}\varepsilon_{dark\_leaves}$	‰	mitochondrial (AOX + COX) isotopic fractionation in leaves	19 ± 1[c]	19 ± 1[c]
$^{18}\varepsilon_{Mehler}$	‰	global Mehler respiration isotopic fractionation	10.8 ± 0.2[d]	10.8 ± 0.2[d]
$^{18}\varepsilon_{photo}$	‰	global photorespiration isotopic fractionation	21.4 ± 1[d]	21.4 ± 1[d]
$^{18}\varepsilon_{resp}$	‰	global terrestrial respiration isotopic fractionation	17.83	17.80
$\delta^{18}O_{p\_amount}$	‰	global precipitation water isotope delta	−6.689	−6.781
$\delta^{18}O_{p}$	‰	global photosynthesis precipitation water isotope delta	−5.530	−5.289
$\delta^{18}O_{vap\_amount}$	‰	global water vapor isotope delta	−12.648	−12.653
$\delta^{18}O_{vap}$	‰	global photosynthesis water vapor isotope delta	−12.483	−12.295
$\delta^{18}O_{leafwater}$	‰	global leaf water isotope delta	5.164 ± 1[e]	5.301 ± 1[e]
$\delta^{18}O_{terr}$	‰	global terrestrial tropospheric isotope delta	23.407 ± 1	23.516 ± 1
$\delta^{18}O_{mar}$	‰	global marine tropospheric isotope delta	25.3 ± 2[f]	25.3 ± 2[f]
$\delta^{18}O_{atm}$	‰	global tropospheric isotope delta	23.88 ± 2	23.95 ± 2

[a] Schlesinger and Andrews, 2000. Note that this estimation is for present-day and here, we assume it was similar during the last glacial period.
[b] Badger et al., 2000.
[c] Landais et al., 2007b.
[d] Helman et al., 2005.
[e] Gillon and Yakir, 2001.
[f] Note that the increase of 1‰ compared to Luz et al. (2014) value accounts for the 1‰ enrichment of the glacial ocean (Waelbroeck et al., 2002).

Table 3. Comparison of isotopic proxy records (speleothem's calcite δ^{18}O) with annual average modeled amount weighted δ^{18}O$_p$. Note that anomalies from Pausata et al. (2011) are calculated from H1 and YD, while anomalies from Lewis et al. (2010) arise from all identifiable δ^{18}O$_c$ excursions.

Core	ID	Region	Latitude	Longitude	Data Δδ^{18}O	Model Δδ^{18}O	Reference
Hulu Cave	XI	China	32.5	119.2	1.4	1.1	Pausata et al. (2011); Lewis et al. (2010)
Songjia Cave	XII	China	31.7	110.5	1.4	1.1	Pausata et al. (2011); Lewis et al. (2010)
Dongge Cave	IX	China	25.3	108.8	1	0.8	Pausata et al. (2011)
Timta Cave	XIII	India	29.8	80.0	3	−3.7	Pausata et al. (2011)
Sanbao Cave	X	China	31.7	110.5	1.2	1.1	Lewis et al. (2010)
Borneo	VI	Indonesia	4.0	114.0	0.8	0.6	Lewis et al. (2010)
Moomi Cave	VIII	Yemen	12.5	54.3	0.9	0.6	Lewis et al. (2010)
Soreq Cave	VI	Israel	31.5	35.0	0.5	0.5	Lewis et al. (2010)
Rio Grande do Norte	II	northeastern Brazil	−5.7	−37.7	−1.6	−0.1	Lewis et al. (2010)
Santana Cave	V	southern Brazil	−24.5	−48.7	−0.8	−0.9	Lewis et al. (2010)
Botuvera Cave	IV	southern Brazil	−27.2	−49.2	−1.1	−1.1	Lewis et al. (2010)
Cave of the Bells	III	North America	31.7	−110.8	−0.8	0.8	Lewis et al. (2010)
Poleva Cave	I	Europe	44.7	21.8	−2	−1.0	Lewis et al. (2010)

Discussion Paper | Discussion Paper | Discussion Paper | Discussion Paper

CPD

11, 2281–2339, 2015

$\delta^{18}O$ variations during a HS

C. Reutenauer et al.

Title Page

Abstract | Introduction

Conclusions | References

Tables | Figures

◄ | ►

◄ | ►

Back | Close

Full Screen / Esc

Printer-friendly Version

Interactive Discussion

Table 4. Comparison of mega-biomes during Heinrich Stadials between pollen reconstructions (references are included in the table) and simulated vegetations (compiled from HS_exp using ORCHIDEE vegetation model). Note that simulated C3 and C4 grasses are merged into 1 mega-biome because pollen-based biome reconstructions do not allow us to distinguish between the two PFTs.

Core	ID	Region	Latitude	Longitude	resolution[a] (yr/sample)	which HS?	Mega Biome distribution pollen data — flora	biome(s) assignation	model results dominant, subdominant biome	Agreement	Reference
Kashiru Bog	1	equatorial Africa	−3.47	29.57	410	HS1	grassland and dry shrubland, savannah and xerophytic scrubland	grasses	tropical forest, grasses	fair	Hessler et al. (2010); Handani et al. (2012)
Lake Tanganyika	2	equatorial Africa	−8.5	30.85	610	HS1	warm temperate mixed forest, savannah and xerophytic scrubland	temperate forest, grasses	grasses, tropical forest	fair	Hessler et al. (2010); Handani et al. (2012)
Lake Masoko	3	equatorial Africa	−9.33	33.75	550	HS1	warm temperate mixed forest, savannah and xerophytic scrubland	temperate forest, grasses	grasses, tropical forest	fair	Hessler et al. (2010); Handani et al. (2012)
Lake Malawi	4	equatorial Africa	−11.29	34.44	200	HS1	savannah and xerophytic scrubland, tropical forest	grasses, tropical forest	grasses	good	Hessler et al. (2010); Handani et al. (2012)
Barombi Mbo	5	equatorial Africa	4.51	9.4	590	HS1	savannah and xerophytic scrubland, tropical forest	grasses, tropical forest	grasses, tropical forest	good	Hessler et al. (2010); Handani et al. (2012)
KS 84-063	6	equatorial Africa	4.4	−4.18	450	HS1	tropical forest, warm temperate mixed forest	tropical forest, temperate forest	tropical forest, grasses	good	Hessler et al. (2010); Handani et al. (2012)
ODP 1078-C	7	equatorial Africa	−11.92	13.4	140	HS1	warm temperate mixed forest, temperate montane forest	temperate forest, boreal forest	bare soil, tropical forest	bad[b] (soil > 90 %)	Hessler et al. (2010); Handani et al. (2012)
GEOB 1023 – Cunene River Mouth	8	equatorial Africa	−17.15	11.02	185	HS1	savannah and xerophytic scrubland, grassland and dry shurbland	grasses	none	none	Hessler et al. (2010); Handani et al. (2012)
Lake Caco	9	South America	−2.97	−43.42	80	HS1	warm temperate mixed forest, tropical forest	temperate forest, tropical forest	bare soil, tropical forest	moderate	Hessler et al. (2010); Handani et al. (2012)
Colonia	10	South America	−23.87	−46.71	710	HS1	savannah and xerophytic scrubland, grassland and dry shurbland	grasses	grasses, temperate forest	good	Hessler et al. (2010); Handani et al. (2012)
La Laguna, Bogota	11	South America	4.92	−74.03	670	HS1	savannah and xerophytic scrubland, grassland and dry shurbland	grasses	bare soil	bad (soil = 100 %)	Hessler et al. (2010); Handani et al. (2012)

Table 4. Continued.

Core	ID	Region	Latitude	Longitude	resolution[a] (yr/sample)	which HS?	Mega Biome distribution			Agreement	Reference
							pollen data		model results dominant, subdominant biome		
							flora	biome(s) assignation			
Fuquene	12	South America	4.92	−74.03	520	HS1	savannah and xerophytic scrubland, temperate montane forests	grasses, temperate forest	bare soil	bad (soil = 100 %)	Hessler et al. (2010); Handiani et al. (2012)
GEOB 3104	13	South America	−3.67	−37.72	670	HS1	temperate montane forest, warm temperate mixed forest	temperate forest	tropical forest, bare soil	bad[b]	Hessler et al. (2010); Handiani et al. (2012)
GEOB 3910-2	14	South America	−4.15	−36.21	125	HS1	savannah and xerophytic scrubland, warm temperate mixed forests	grasses, temperate forest	tropical forest, bare soil	bad[b]	Hessler et al. (2010); Handiani et al. (2012)
MD03-2622	15	South America	10.71	−65.17	420	HS3, HS4, HS5	montane forest, semi-deciduous forest, savannah (except HS4)	temperate forest, grasses	none	none	Hessler et al. (2010); Handiani et al. (2012)
17 962	16	Australasia	7.18	112.08	370	HS4	tropical forest	tropical forest	tropical forest, grasses	good	Harrison and Sanchez-Goni (2010)
18 300	17	Australasia	4.35	108.65	526	HS4	tropical forest	tropical forest	tropical forest, grasses	good	Harrison and Sanchez-Goni (2010)
18 323	18	Australasia	2.78	107.88	420	HS4	tropical forest	tropical forest	tropical forest, grasses	good	Harrison and Sanchez-Goni (2010)
Lake Wangroom	19	Australasia	−38.35	142.6	362	HS4	herbaceous and shrublands	grasses	temperate forest, tropical forest	bad	Harrison and Sanchez-Goni (2010)
Tyrendarra Swamp	20	Australasia	−38.2	141.76	337	HS4	herbaceous and shrublands	grasses	temperate forest, tropical forest	bad	Harrison and Sanchez-Goni (2010)
Lake Surprise	21	Australasia	−38.06	141.92	345	HS4	herbaceous and shrublands	grasses	temperate forest, tropical forest	bad	Harrison and Sanchez-Goni (2010)
Kohuora	22	Australasia	−36.57	174.52	375	HS4	herbaceous and shrublands	grasses	temperate forest, tropical forest	bad	Harrison and Sanchez-Goni (2010)
Native Companion Lagoon	23	Australasia	−27.68	153.41	655	HS4	tropical forest and open forest, woodland	tropical forest, temperate forest	bare soil, temperate forest	moderate	Harrison and Sanchez-Goni (2010)
Ioannina 284	24	Europe	39.75	20.85	325	HS4	grassland and dry shrubland	grasses	boreal forest, grasses	fair	Fletscher et al. (2010)
Megali Limni	25	Europe	39.1	26.32	150	HS4	grassland and dry shrubland with 40 % xerophytic steppe elements	grasses	grasses, boreal forest	good	Fletscher et al. (2010)
Lago Grande di Monticchio	26	Europe	40.93	15.62	210	HS4	grassland and dry shrubland with 40 % xerophytic steppe elements	grasses	boreal forest, grasses	fair	Fletscher et al. (2010)
MD04-2845	27	Europe	45.35	−5.22	540	HS3	grassland and dry shrubland	grasses	none	none	Fletscher et al. (2010)
MD99-2331	28	Europe	41.15	−9.68	390	HS4	grassland and dry shrubland	grasses	none	none	Fletscher et al. (2010)

Table 4. Continued.

Core	ID	Region	Latitude	Longitude	resolution[a] (yr/sample)	which HS?	Mega Biome distribution pollen data — flora	Mega Biome distribution pollen data — biome(s) assignation	model results — dominant, subdominant biome	Agreement	Reference
MD95-2039	29	Europe	40.58	−10.35	300	HS4	grassland and dry shrub-land	grasses	none	none	Fletscher et al. (2010)
MD95-2042	30	Europe	37.8	−10.17	360	HS4	grassland and dry shrub-land with 40 % xerophytic steppe elements	grasses	none	none	Fletscher et al. (2010)
ODP site 976	31	Europe	36.2	−4.3	240	HS4	grassland and dry shrub-land with 40 % xerophytic steppe elements	grasses	bare soil, boreal forest	bad (soil > 90 %)	Fletscher et al. (2010)
MD95-2043	32	Europe	36.13	−2.62	260	HS4	grassland and dry shrub-land with 40 % xerophytic steppe elements	grasses	bare soil, boreal forest	bad (soil > 90 %)	Fletscher et al. (2010)
Khoe	33	Japan	51.34	142.14	750	HS4	cold deciduous and evergreen conifer forest	boreal forest	boreal forest, grasses	good	Takahara et al. (2010)
Kenbuchi	34	Japan	44.05	142.38	250	HS1, HS2	cold deciduous forest	boreal forest	boreal forest, grasses	good	Takahara et al. (2010)
MD01-2421	35	Japan	36.02	141.77	150	HS4	cold evergreen conifer forest	boreal forest	boreal forest, temperate forest	good	Takahara et al. (2010)
Lake No-jiri	36	Japan	36.83	138.22	100	HS4	increase of cold evergreen conifer forest within cool conifer forest	temperate forest, boreal forest	none	none	Takahara et al. (2010)
Lake Biwa	37	Japan	35.22	136	300	HS4	increase of cool conifer forest within temperate conifer forest	temperate forest	boreal forest, temperate forest	fair	Takahara et al. (2010)
Kamiyoshi Basin	38	Japan	35.1	135.59	800	HS4	increase of cool conifer within temperate conifer forest, and deciduous broadleaf forest	temperate forest	boreal forest, temperate forest	fair	Takahara et al. (2010)
Toushe Basin	39	Japan	23.82	120.88	300	HS4	temperate deciduous or warm temperate evergreen forest	temperate forest	boreal forest, temperate forest	good	Takahara et al. (2010)
Fargher Lake	40	North-America	45.88	−122.58	270	HS4	boreal forest	boreal forest	none	none	Jimenez-Moreno et al. (2010)
Carp Lake	41	North-America	45.91	−120.88	630	HS4	open temperate and pine forest	temperate forest	none	none	Jimenez-Moreno et al. (2010)
Little Lake	42	North-America	44.16	−123.58	260	HS4	boreal-temperate forest	boreal forest, temperate forest	none	none	Jimenez-Moreno et al. (2010)
W8709A-13PC	43	North-America	42.25	−127.66	430	HS4	boreal forest with decrease in heterophyla	boreal forest	none	none	Jimenez-Moreno et al. (2010)
EW-9504-17PC	44	North-America	42.23	−125.81	460	HS1, HS2, HS3	warm temperate	temperate forest, tropical forest	none	none	Jimenez-Moreno et al. (2010)
ODP 893A	45	North-America	34.28	−120.03	220	HS4	open temperate forest	temperate forest	temperate forest, bare soil	good	Jimenez-Moreno et al. (2010)

Title Page

Abstract | Introduction

Conclusions | References

Tables | Figures

◄ | ►

◄ | ►

Back | Close

Full Screen / Esc

Printer-friendly Version

Interactive Discussion

Table 4. Continued.

Core	ID	Region	Latitude	Longitude	resolution[a] (yr/sample)	which HS?	Mega Biome distribution pollen data flora	pollen data biome(s) assignation	model results dominant, subdominant biome	Agreement	Reference
Bear Lake	46	North-America	41.95	−111.3	680	HS4	xerophytic shrubland	grasses	grasses	good	Jimenez-Moreno et al. (2010)
Camel Lake	47	North-America	30.26	−85.01	300	HS4	temperate forest with increase in southeastern pine forest	temperate forest	boreal forest, temperate forest	fair	Jimenez-Moreno et al. (2010)
Lake Tulane	48	North-America	27.58	−81.5	480	HS4	southeastern pine forest, florida scrub	grasses, temperate forest	bare soil, temperate forest	moderate	Jimenez-Moreno et al. (2010)

[a] Sampling resolutions of the MIS where vegetation changes occur. Mean sampling resolution is 393 yrs.
[b] Similar to Handiani et al. (2012) model results.
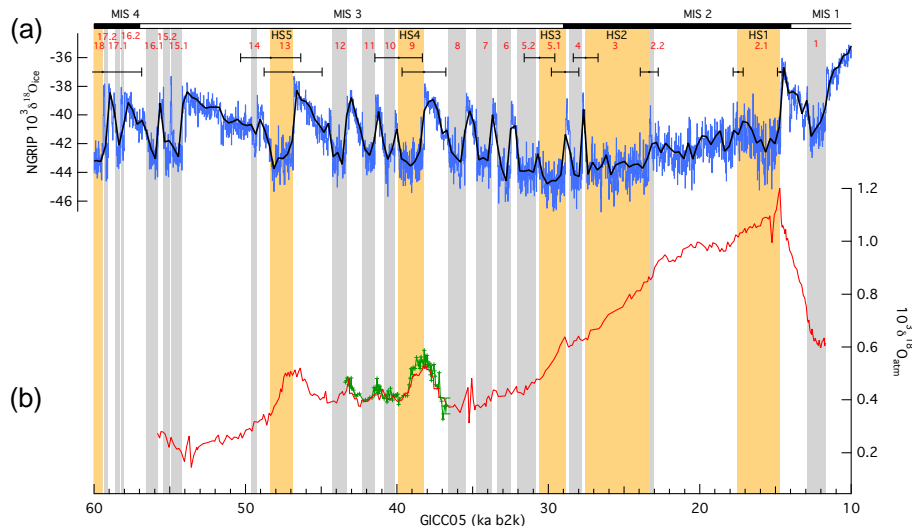
Figure 1. Greenland Stadials (GS) and Heinrich Stadials (HS) during the last glacial period. Red numbers indicate GS and black labels HSs. **(a)** Black line: NGRIP δ^{18}O, ‰, on the GICC05 timescale back to 60 ka b2k. **(b)** Red line: Siple Dome on GICC05 timescale. The transfer of Siple Dome atmospheric δ^{18}O on the GICC05 chronology is achieved using the Siple Dome gas age scale compatible with the GICC05 chronology (Guillevic, 2013), based on match points between Siple Dome methane variations (Brook et al., 2005; Ahn et al., 2012) (depth point) and NEEM methane variations (Chappellaz et al., 2013) (GICC05 gas age point). A linear interpolation is then performed between match points to calculate the Siple Dome gas age. Green line: NEEM atmospheric δ^{18}O, ‰ (±0.03‰) (Guillevic et al., 2014). Colored areas: GSs. Grey: GS with no major Heinrich event. Orange: HS1, HS2, HS3, HS4, HS5 and end of HS6: GSs with a major Heinrich event. Black error bars indicate HS onset and end uncertainty (2σ), based on Rasmussen et al. (2013) Maximum Counting Error (MCE). Top (right to left): black and white vertical bar indicate Marine Isotope Stage 1 to 4.
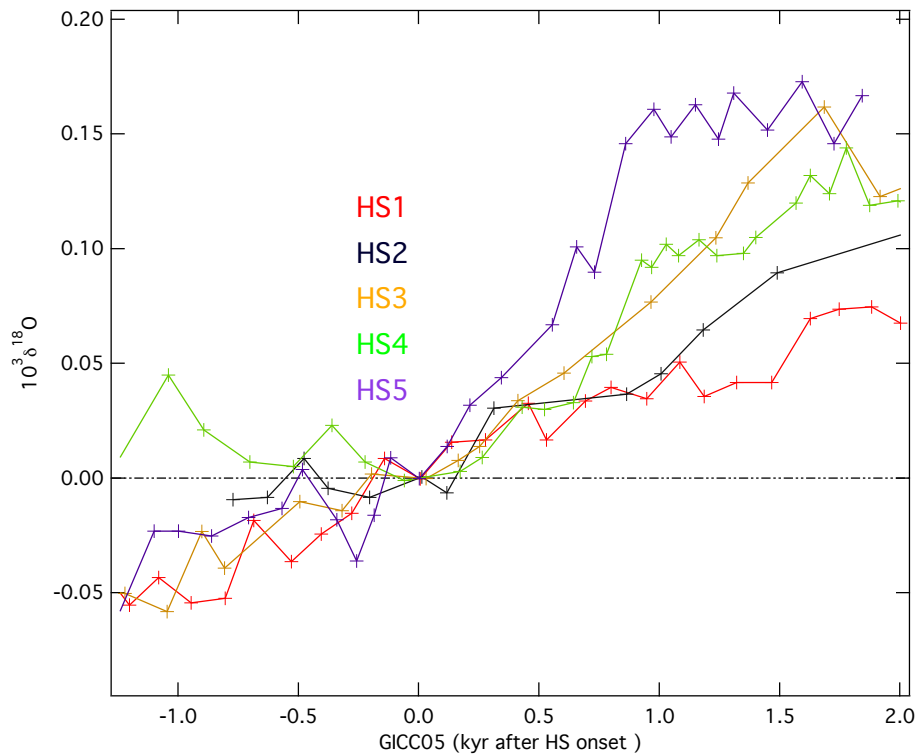
Figure 2. Evolution of Siple Dome atmospheric oxygen $\delta^{18}O$ (Severinghaus et al., 2009) during Heinrich Stadial on the GICC05 timescale.
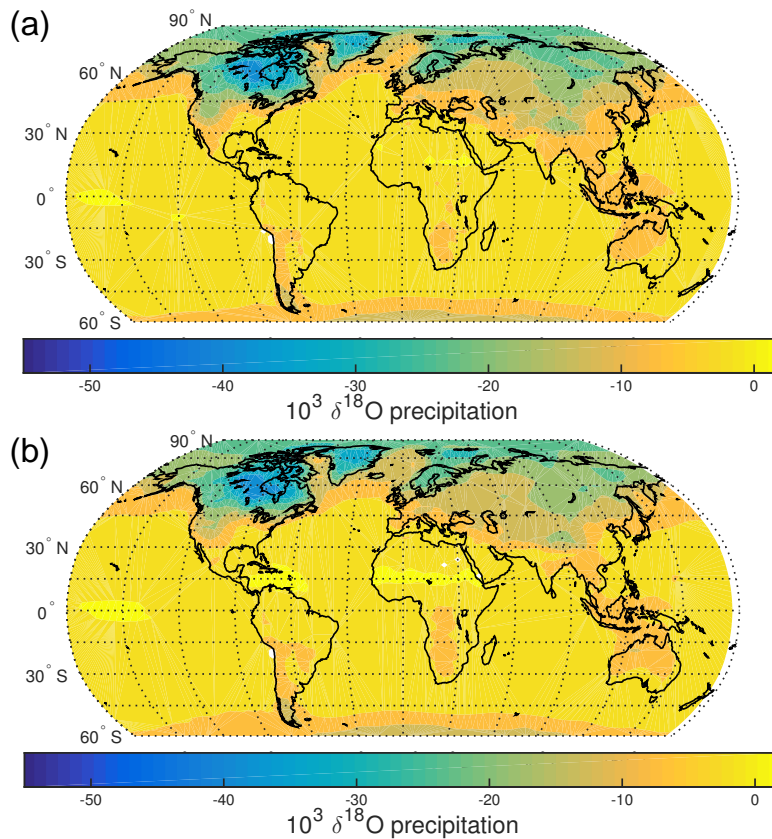
Figure 3. Amount weighted annual-mean δ^{18}O of precipitation for **(a)** LGM_ctrl and **(b)** HS_exp experiments obtained with LMDZ-iso.

Title Page

Abstract | Introduction

Conclusions | References

Tables | Figures

|◄ | ►|

◄ | ►

Back | Close

Full Screen / Esc

Printer-friendly Version

Interactive Discussion
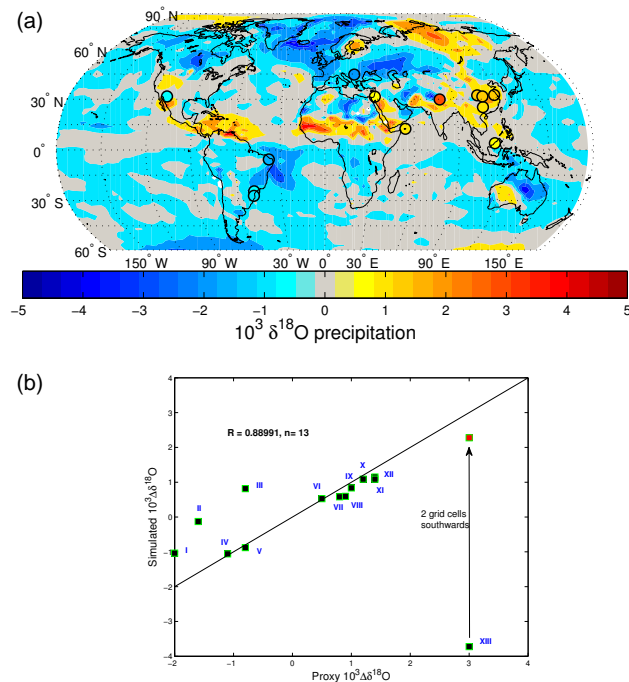
Figure 4. (a) Model–data comparison of precipitation anomaly during HS compared to LGM. Data represent speleothem's calcite δ^{18}O from various locations (see Table 3 for details). **(b)** Comparison of reconstructed HS precipitation anomaly $\Delta\delta^{18}$O from selected proxies shown in a and simulated $\Delta\delta^{18}$O$_p$ anomaly ($R = 0.89$, $n = 13$). Note that the correlation is done with point XIII corrected, as we assume a bias in the model. Refer to Table 3 for details on reconstructed precipitation. Points falling on the line depict the same anomaly in the reconstruction and the simulation. Note that Timta and Dongge (Wang et al., 2005) cave δ^{18}O$_c$ were estimated from the YD excursion, sometimes called H0 and characterized by a large freshwater input in the NA (Pausata et al., 2011).
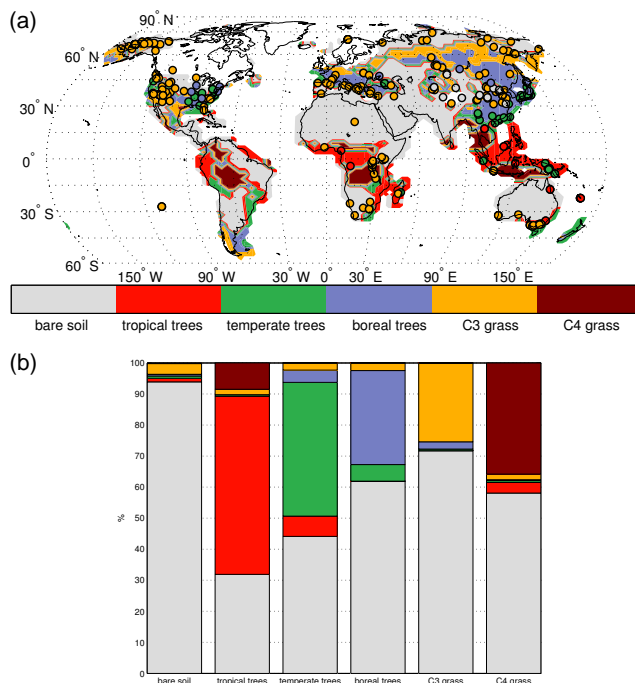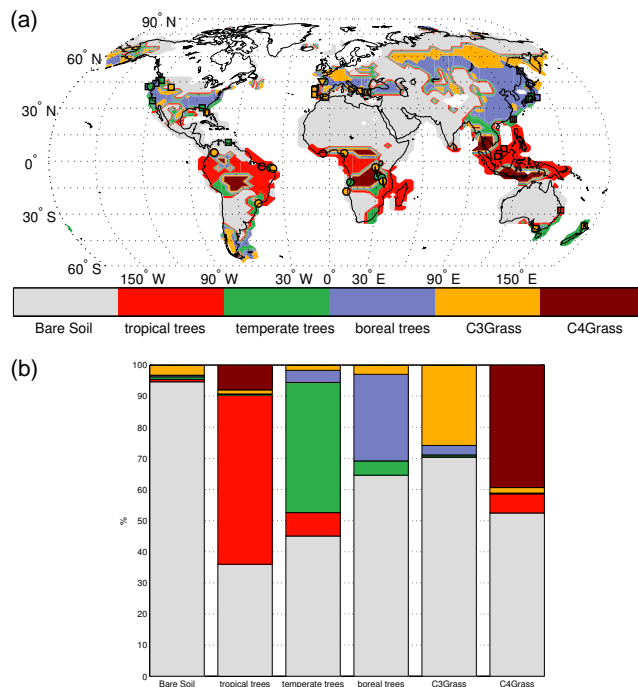
Figure 5. (a) Model–data comparison of mega-biome distribution for LGM_ctrl based on dominant PFT type simulated by ORCHIDEE. For each grid-cell, the fraction of bare soil, tropical forests, temperate forests, boreal forests, C3 and C4 grasses is considered. The type covering the greatest cell fraction is the dominant type. Note that dominant bare soil fraction denotes more than 80 %. Circles denote LGM mega-biomes inferred from pollen and plant macrofossil records compiled by the BIOME6000 project. Refer to Table 4 to see how PFT's simulated by ORCHIDEE have been assigned to the mega-biomes mapped in this figure. **(b)** Detail of the averaged vegetation composition in grid cells occupied by a dominant mega-biome for LGM_ctrl.

Figure 6. (a) Model–data comparison of mega-biome distribution for HS_exp based on dominant PFT type simulated by ORCHIDEE. For each grid-cell, the fraction of bare soil, tropical forests, temperate forests, boreal forests, C3 and C4 grasses is considered. The type covering the greatest cell fraction is the dominant type. Note that dominant bare soil fraction denotes more than 80 %. Circles denote HS_exp mega-biomes inferred from pollen and plant macro-fossil records compilation. Refer to Table 4 to see how PFT's simulated by ORCHIDEE and reconstructed vegetation have been assigned to the mega-biomes mapped in this figure. **(b)** Detail of the averaged vegetation composition in grid cells occupied by a dominant mega-biome for HS_exp.

Title Page

Abstract | Introduction

Conclusions | References

Tables | Figures

|◄ | ►|

◄ | ►

Back | Close

Full Screen / Esc

Printer-friendly Version

Interactive Discussion
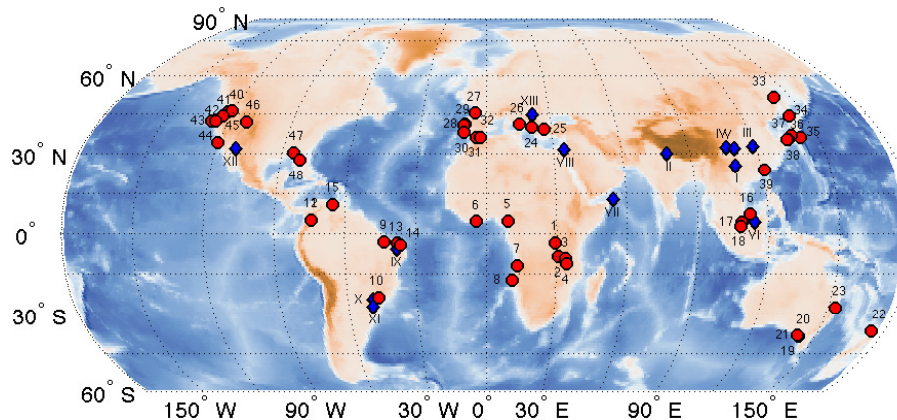
Figure 7. Location of marine and terrestrial paleoarchives sites included in the model–data comparison. Blue diamonds denote speleothem's calcite $\delta^{18}O$ and red circles denote pollen records. Arabic and roman numbers displayed in the map identify the location of the paleoarchives listed in Tables 3 (hydrology) and 4 (vegetation) for site names, references and further details.
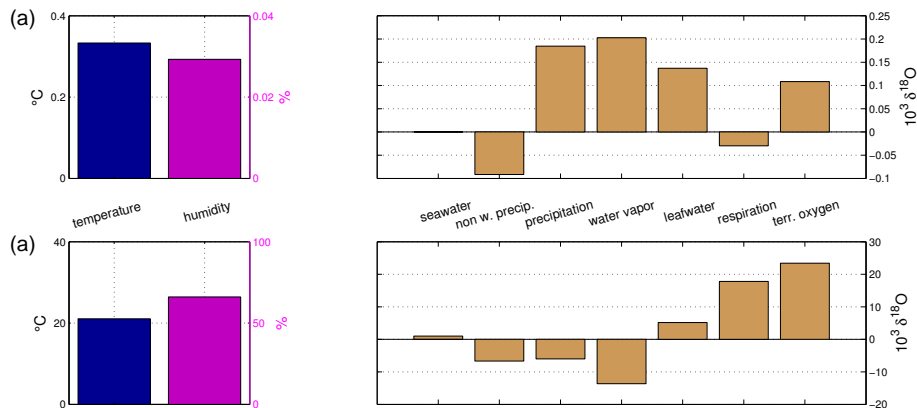
Figure 8. Evolution of the main simulated factors controlling atmospheric δ^{18}O. Note that all variables are oxygen production weighted, i.e. integrated over vegetated areas, if not stated with "non w.". **(a)** Left panel: HS_exp – LGM_ctrl anomalies of temperature and relative humidity. Right panel: (left to right) HS_exp – LGM_ctrl anomalies of seawater δ^{18}O, amount weighted precipitation δ^{18}O, precipitation δ^{18}O (δ^{18}O$_p$), water vapor δ^{18}O, leaf water δ^{18}O (δ^{18}O$_{lw}$), respiratory isotope fractionation ($-^{18}\varepsilon_{resp}$) and terrestrial contribution to atmospheric δ^{18}O (δ^{18}O$_{terr}$). **(b)** LGM_ctrl values of same relevant factors as in **(a)** in δ^{18}O$_{terr}$ budget. Note that plotted respiratory isotope fractionation anomaly is inverted as respiration is an oxygen uptake process.
δ^{18}O$_{lw}$ is controlled by δ^{18}O$_p$, temperature and relative humidity as described by Eq. (4). Combined with $^{18}\varepsilon_{resp}$ as described in Eq. (3), one obtain δ^{18}O$_{terr}$.
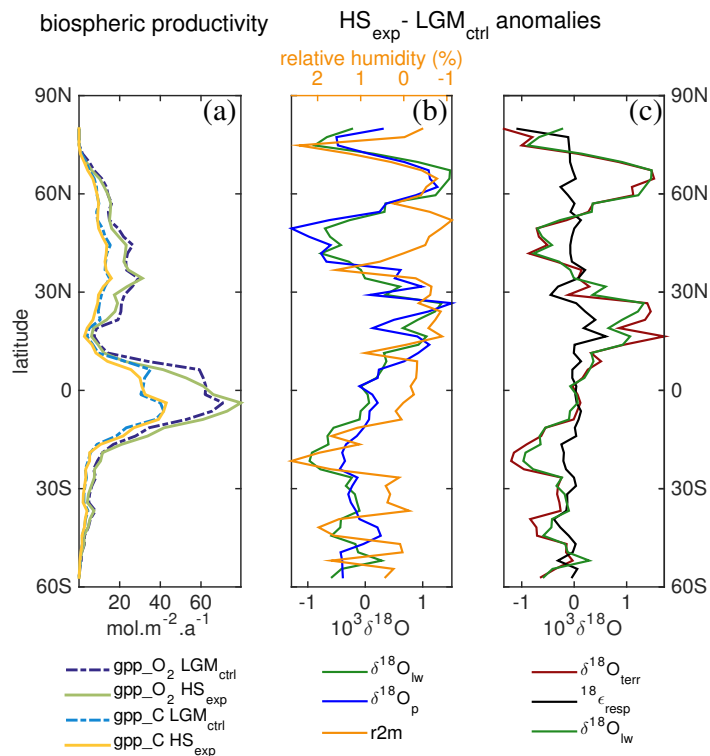
Figure 9. (a) Zonal annual mean of gross primary productivity expressed in terms of carbon (GPP_C) and oxygen (GPP_O$_2$) annual molar fluxes for LGM_ctrl and HS_exp, resp. **(b)** Zonal annual mean anomalies of δ^{18}O$_{lw}$, δ^{18}O$_p$ and relative humidity (be aware of its inverted x axis). **(c)** Zonal annual mean anomalies for $-^{18}\epsilon_{resp}$, δ^{18}O$_{lw}$ and δ^{18}O$_{terr}$. Note that all variables of panels **(b)** and **(c)** are oxygen production (GPP_O$_2$) weighted.
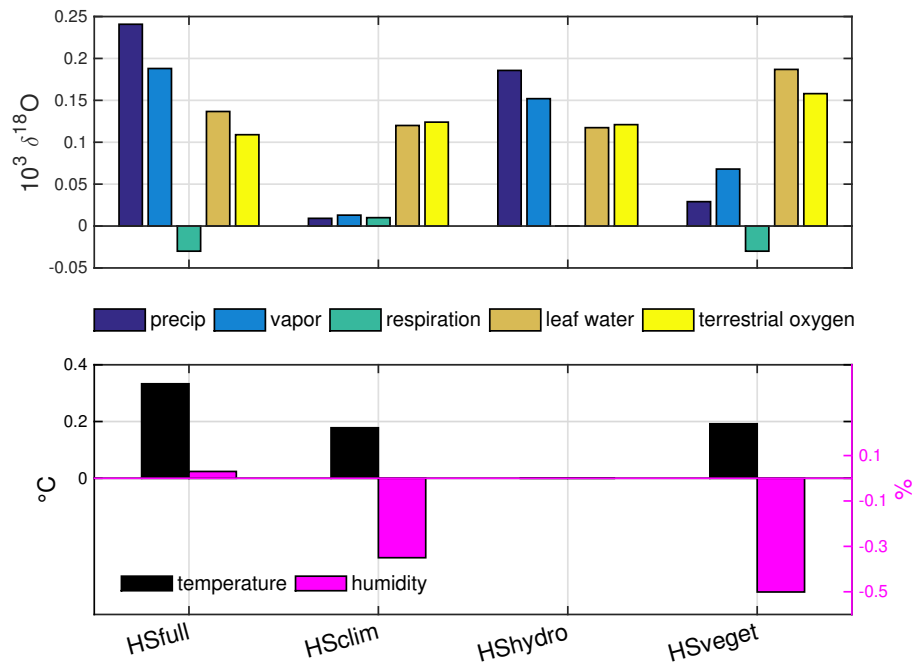
Figure 10. Summary of sensitivity study experiments. HSfull uses same settings as HS_exp, while HSclim, HShydro and HSveget experiments are identical to LGM_ctrl, except for meteoric waters isotopic composition, climatic conditions or vegetation production and distribution, respectively, originating from HS_exp. For each of the experiments are presented annual mean anomaly (experiment – LGM_ctrl) of oxygen production weighted temperature, relative humidity, $\delta^{18}O_p$, water vapor δ^{18}O, $\delta^{18}O_{lw}$, $^{18}\varepsilon_{resp}$ and $\delta^{18}O_{terr}$.